BRIMROSE Technology Corporation
P.O. Box 616, 19 Loveton Circle, Sparks, Maryland 21152-9201
Phone: 410-472-2600; Fax: 410-472-7960; www.brimrosetechnology.com

Magnesium and Manganese Silicides For Efficient And Low Cost Thermo-Electric Power Generation

Phase I Grant - DE-SC0009453

(Purchase Request or Funding Document No.: 13SC001301)

EXECUTIVE SUMMARY

Thermoelectric Power Generation (TEPG) is the most efficient and commercially deployable power generation technology for harvesting wasted heat from such things as automobile exhausts, industrial furnaces, and incinerators, and converting it into usable electrical power. TEPGs offer distinct advantages over other technologies such as: no moving parts, low-weight, modularity, high power density, low amortized cost, and long service life. However, widespread commercial integration of TEPG has been impeded for several reasons, the most crucial being the need for materials with high TE figure of merit (ZT) that also have long life, are low cost and (preferably) light in weight. We investigated the materials magnesium silicide (Mg_2Si) and manganese silicide (MnSi) for TEPG. Compared with other TE materials operating in the same temperature range, $MgSi_2$ and MnSi are environmentally friendly, have constituent elements that are abundant in the earth's crust, non-toxic, lighter and cheaper. To date, Japanese researchers are the only ones in the world who are commercially producing these promising materials and investigating Ohmic contact technology to build TEPG modules from them.

The initiatives that we bring to this work are key to the development of device quality TE material. The first is that Brimrose has developed special procedures for obtaining extremely high-purity Mn and Mg elemental sources and novel processes to synthesize stoichiometric silicide materials. With high purity sources and control of stoichiometry and dopant concentration, it is easier to optimize ZT. The second is the use of the field assisted-spark plasma sintering technology (FAST) developed by our collaborators at Penn State University. This novel technique is used to produce high quality, uniform, bulk nano-structured TE materials. Nanostructuring leads to a decrease in thermal conductivity and therefore improvement in ZT. Furthermore, the manufacturing of nano-composites using FAST is a rapid production technique that is amenable to large scale production.

In Phase I, we successfully produced Mg_2Si and MnSi material with good TE properties. We developed a novel technique to synthesize Mg_2Si with good crystalline quality, which is normally very difficult due to high Mg vapor pressure and its corrosive nature. We produced n-type Mg_2Si and p-type MnSi nanocomposite pellets using FAST. X-ray diffraction measurements confirmed that the materials were stoichiometric, and optical micrographs revealed they were fully dense with very little porosity. Several TEPG devices were fabricated. Measurements of resistivity and voltage under a temperature gradient indicated a Seebeck coefficient of roughly 120 μV/K on average per leg, which is quite respectable. Results indicated however, that issues related to bonding resulted in high resistivity contacts. Determining a bonding process and bonding material that can provide Ohmic contact from room temperature to the operating temperature is an essential part of successful device fabrication. Work continues in the development of a process for reproducibly obtaining low resistance electrical contacts. Within the Phase I time frame we have successfully achieved TE results similar to those reported in the literature from the Japanese researchers. Our results indicate that we are on track to develop materials with ZT on the order of 1.6 or higher.

DOE/11182013-Final

Magnesium and Manganese Silicides For Efficient And Low Cost Thermo-Electric Power Generation

Final Report

February 19, 2013 – November 18, 2013

Brimrose Technology Corporation
19 Loveton Circle
Sparks, Maryland 21152-9201

Key Personnel
Brimrose Technology Corporation

Dr. Sudhir B. Trivedi
Dr. Susan W. Kutcher
Mr.Cory Rosemeier
Mr. David Mayers

Dr. Jogender Singh
The Pennsylvania State University
Subcontractor

November 18, 2013

Prepared for

THE U.S. DEPARTMENT OF ENERGY
Under Grant Award – DE-SC00009453

Report contains "No proprietary information"

Magnesium and Manganese Silicides For Efficient And Low Cost Thermo-Electric Power Generation

Phase I Grant - DE-SC0009453

(Purchase Request or Funding Document No.: 13SC001301)

TABLE OF CONTENTS

	Page
Executive Summary	
Cover Page	i
Table Of Contents	ii
List Of Figures	iii
List Of Tables	**v**
1. Introduction	1
2. Background and Rational	1
2.1 Background on Thermoelectric Materials Issues	2
2.2 Why Magnesium Silicide and Manganese Silicide	2
3. Summary Of Results	4
4. Results and Discussion	5
4.1 Materials Synthesis and XRD	5
4.2 Sintering of Nanopowders	13
4.3 Preparation of N and P-Type Legs	21
4.4 Electrical Measurements on Legs	24
4.5 Device Fabrication and Characterization	26
4.6 Investigation of Thermal Management	34
5. Conclusion and Future Plans	36
6. References	38

LIST OF FIGURES

Figure		Page
1	Mg-Si phase diagram [25]	6
2	Syntheses assembly and its elements	8
3	The products of syntheses	9
4	Remelted Mg_2Si Ingot	9
5	Remelted $MnSi_{(1.74)}$ Ingot	10
6	Ingot of remelted Magnesium Silicide chunks from Yasanuga, Japan	10
7	Optimized as Synthesis of Mg_2Si:Sb ingot	12
8	Relationship between hold temperature, applied pressure and resulting grain size in Field Assisted Sintering Technology [27]	13
9	X-ray Diffraction pattern of Sb doped Mg_2Si nanopowder	16
10	X-ray Diffraction pattern of sintered bulk nano-composite of Sb doped Mg_2Si	16
11	X-ray Diffraction pattern of sintered bulk nano-composites of Sb doped Mg_2Si with added nickel (Ni)	17
12	Reference x-ray diffraction pattern of Mg_2Si at various stoichiometry from Kim et al [32]	17
13	X-ray Diffraction pattern of MnSi nanopowder	18
14	Reference x-ray diffraction pattern of MnSi at various stoichiometry [18]	18
15	Photograph of FAST sintered nanocomposites of Mg_2Si and MnSi produced during this work	19
16	Optical micrographs of the Japanese Mg_2Si material at 200X and 1000X. This sample is nearly fully dense with scattered pores in 2-8 μm range	19
17	Optical micrographs of Japanese MnSi at 200X and 1000X, This sample has pores in 1-5 μm range	20

18	Optical micrographs of Brimrose Mg_2Si at 200X and 1000X. This sample is almost fully dense with little porosity	20
19	Optical micrographs of Brimrose MnSi at 200X and 1000X. This nearly fully dense with isolated large pores (5-15 μm)	21
20	Experimental Setup for Nickel plating	22
21	Photograph showing typical nickel plated sintered pallet	23
22	Photographs of Mg_2Si and MnSi sintered material cut into legs in preparation for fabrication of a thermoelectric device	23
23	Photograph of resistivity measurement setup and a close-up of the sample holder	24
24	Device Fabrication Setup	27
25	Silicide based TEPG devices fabricated using setup shown in Figure 24	27
26	Method used to characterize TEPG devices	28
27	Set-up for measurement of properties of TEPG device	29
28	Close up view of the set-up shown in Figure 27	29
29	Plot of the voltage drop across the standard resistance versus current for Sample #1	30
30	Combined Seebeck Determination for Sample #1	32
31	Combined Seebeck Determination for Sample #3	33
32	Combined Seebeck Determination for Sample #4	34
33	Thermal Diffusivity of copper alloy with various volume fractions of carbon nanotubes (CNTs)	35
34	Thermal conductivity of Al with various volume fraction of TEPG flakes and corresponding cross section microstructure	36

LIST OF TABLES

Table

1	Table summarizing the bulk nanostructured samples prepared by FAST	15
2	Electrodeposition of Nickel: optimized deposition conditions	22
3	Resistance and Resistivity measurements for Mg_2Si	25
4	Resistance and Resistivity measurements for MnSi	25
5	Measurements on Device #1	30
6	Open Circuit Voltage vs Delta T for Sample #1	31
7	Open Circuit Voltage vs Delta T for Sample #3	32
8	Open Circuit Voltage vs Delta T for Sample #4	33

1. Introduction

The current DOE program aims to convert otherwise wasted heat from automobiles into useful electrical power. Government agencies like DOE, DOD and automobile industries have identified conversion of waste heat from vehicular exhaust to electric power as one of their focuses. Thermoelectric Power Generation (TEPG) is the most efficient and commercially deployable power generation technology that can convert otherwise wasted heat from automobiles (and other sources) into useful electrical power. A thermoelectric power generator is a solid state device that provides direct energy conversion from thermal energy (heat) due to a temperature gradient into electrical energy based on the "Seebeck effect". Thermoelectric power generators offer several distinct advantages over other technologies such as: no moving parts, low-weight, modularity, silence, high power density, low amortized cost, and long service life with no required maintenance.

However, the widespread commercial integration of TEPG has been impeded for several reasons:

- Foremost, is their relatively low conversion efficiency (typically ~5%). This has been a major cause in restricting their use to specialized fields where reliability is a major consideration and cost is not. Efficiency is determined primarily by the material properties that contribute to ZT, the "figure-of-merit" for TE material.
- Second, issues with the device design (size, shape, high temperature ohmic contacts, thermal management, electronics) and efficient production (low cost, high yield, producibility) need to be optimized. For instance, approaches for efficient passive thermal management and control of heat dissipation (i.e. heat sinking) have not been completely engineered. There are also device-related problems associated with preventing inter-diffusion and extending the service lifetime of high temperature Ohmic contacts.
- And the third reason that TEPG technology has not been utilized in the commercial marketplace is that strategies for protection against environmental degradation are needed to maintain the chemical, mechanical and electronic integrity of the TE materials and devices while operating at high temperature for the entire service lifetime.

All of these issues must be addressed in order to make TEPG a viable method of power generation compatible with the main stream energy harvesting technologies, and we deal with each one in the proposed program.

2. Background and Rationale

In the proposed overall Phase I and Phase II work, we will address the material, device and manufacturing issues with the goal of producing economically viable TEPG devices. Before tackling the device and manufacturing issues, the basic science/technology issues at various component levels must be addressed.

2.1 Background on Thermoelectric Material Issues

The most crucial issue is the development of materials with high thermoelectric figure of merit (Z), having long life, low cost and preferably light weight. The TE figure of merit is defined as

$$Z = \frac{S^2\sigma}{\lambda}$$

Where S is the Seebeck coefficient (also, known as the power factor), σ is the electrical conductivity and λ is the thermal conductivity. The value used to compare TE materials is expressed as ZT where T is the absolute temperature in degrees Kelvin. From the time that the Seebeck effect was discovered in 1821 until early 2000, researchers were not able to produce bulk material with ZT beyond the value of 1 because the various transport properties involved are interrelated in unfavorable ways [1, 2]. For example, improving electrical conductivity generally also increases the thermal conductivity and therefore, their ratio does not increase.

Most approaches leading to improvements in ZT have for the most part focused either on (a) suppressing phonon transport, which reduces the lattice thermal conductivity [3-5] or (b) enhancing the electronic transport properties via carrier filtering [6, 7], resonant level doping [8, 9], and/or and band structure engineering [10, 11]. Low dimensional and nanostructured thermoelectrics present a possible route for utilizing both effects [12, 13]. As a result of these developments in nanostructuring, TEPG technology is showing greater promise of being efficient and commercially deployable power generation technology using variety of waste heat sources such as automobiles [14].

The goal of Phase I program was to produce TE material that: (1) Can operate at high temperature with a conversion efficiency greater than 10% (from typical automotive temperature differences); (2) Has a long life with minimal or no degradation; and (3) Has higher power density than what is currently available. To achieve these characteristics, the following material requirements are necessary: the material must be capable of operating from about 500-1000K; it must have low lattice thermal conductivity κ_L, high values of ZT (greater than 1 and ultimately between 1.6 and 2.0), and good mechanical properties. Furthermore, it must contain readily available inexpensive raw materials that are environmentally friendly. This means steering away from tellurium based TEPG materials (which are the most understood and developed materials operating in mid-temperature range of 500-800 K) because of the toxicity of Te along with the fact that they believe there is not enough supply of tellurium in the earth's crust to meet the needs for TEPG.

2.2 Why Magnesium Silicide and Manganese Silicide?

We investigated the environmentally friendly materials magnesium silicide (Mg_2Si) and manganese silicide (MnSi). These materials were recently identified as possible high-performance TE materials for the temperature range 500-1000K [15-17]. During Phase I, we used Mg_2Si as the n-type material and MnSi as the p-type material for the fabrication of the

thermo-electric devices/modules. As grown Mg_2Si is n-type but does not have required carrier concentration. Therefore, we considered well known antimony (Sb) doped Mg_2Si as the n-type TEPG material. We also explored doping Mg_2Si with Silver (Ag) to produce p-type Mg_2Si. Our aim for Phase II will be to have both n-type and p-type legs of the same material providing longevity (by alleviating thermal expansion mismatch issues during temperature cycling and long term operation) to TEPG device.

Tellurium based TE materials, which are the most understood and developed materials operating in mid-temperature range of 500-800 K, are considered toxic and many believe there is not enough supply of tellurium in the earth's crust to meet the needs for TEPG. On the other hand, silicon, magnesium and manganese can all be obtained from the earth in large quantities. Also, compared to compound telluride-based materials (e.g., PbTe) and skutterudite-based materials (e.g., $CoSb_3$), the proposed silicide-based material alloys (e.g., Mg-Si, Mn-Si) can be used in the high temperature ranges where the Te based materials will fail by decomposition, sublimation, or even melting. Magnesium and manganese silicides are also much lighter and lower cost materials compared to Skutterudite and PbTe materials. Overall, compared with other TE materials operating in the same conversion temperature range, $MgSi_2$ and MnSi are environmentally friendly materials, have constituent elements that are abundant in the earth's crust, are non-toxic, lighter and cheaper. These advantages have made these materials very promising alternatives for commercial TEPG.

A key advantage that the Brimrose approach brings to this DOE initiative is that Brimrose has developed, under DOD funding, special procedures for obtaining extremely high-purity Mn and Mg elemental sources. The key to optimized ZT is control of the doping concentration in the materials. With high purity sources, that control is straightforward. Moreover, silicon-based TEPG legs will self-protect by the formation of dense SiO_2 layers on the outer surface. No inert gas or aero-gel encapsulation is required to extend the operational lifetime of these power-generating modules.

The ultimate goal of this work is to produce the Mg-Si and Mn-Si alloys with ZT values > 1.6. The current published values of ZT for these materials are in the range 0.8 to 1.1 and have optimum operating temperature range of 500-1000K [3,4]. Recent developmental research has shown that nanostructuring should lead to a decrease in thermal conductivity and therefore improvement in ZT, particularly at low temperatures where boundary scattering of phonons is most effective [18-20]. Another approach is to introduce a high number of interfaces within a material. The best example of such interfaces is the simple grain boundary. The reduction of thermal conductivity by grain boundary scattering is well known. However, the advent of technology to produce uniform nanostructured material is new.

Brimrose, in collaboration with Dr. Jogender Singh at ARL/Penn State University, has successfully produced the needed bulk nanostructured materials from the nano powders, using, field assisted-spark plasma sintering technology (FAST) [21,22]. Dr. Singh's lab at ARL/Penn State University is one of the few institutions in the country with availability of two FAST units, one amenable to research and development activities and other amenable to production. In collaboration with ARL/PSU we have successfully produced sintered magnesium and manganese silicides using FAST.

3. Summary of Results

During Phase I of this research, we spent considerable time extensively investigating the **procedures for producing high quality TE material**. We produced nano-powders of Mg_2Si and MnSi, by ball milling and consolidated them into bulk nano-composite form using FAST. The bulk nano-composite materials were ground and polished on both sides to the required thickness (6 mm) and electrochemically coated with a 2 μm layer of nickel. The nickel coated sintered material was then cut into 3mm X 3mm X 6mm n-type and p-type legs to fabricate a thermoelectric devices. We measured the resistance of each leg using the four-probe technique and selected suitable leg pairs to fabricate several TEPG devices. These devices showed good thermoelectric characteristics.

We had synthesized Mg_2Si in-house as well as procured commercially available Mg_2Si from the Japan, the only known commercial source of TEPG grade silicide materials. Our Phase I study indicated that our in-house material had better chemical stability and could be produced at significantly lower cost.

Next, during Phase I we addressed the formation of alloy based Ohmic contacts on TEPG legs. Current braze-based electrical contacts typically involve a mixture of elemental aluminum and silicon, which are known to chemically react with TE component materials. In an effort to improve the TE properties while also making the TEPG device more able to withstand the harsh environments of high temperatures and continuous temperature cycling, we have employed novel high temperature electrical contact materials during the fabrication of the TE devices. This electrical contact material was developed by Brimrose in collaboration with Dr. Patrick Taylor of ARL [23]. The new electrical contact metallurgy appears to be a highly promising baseline approach from which long-term stability and reliability can be optimized.

As mentioned earlier, we had successfully developed nickel coatings for Mg_2Si and MnSi material using electrochemical technique. This coating about 2-3 μm thick can also act as blocking contacts and help in making high temperature Ohmic contacts to TEPG devices using the technique developed in collaboration with ARL [23]. The details of forming Ohmic contacts are given later in the report

Finally during Phase I, **we investigated the novel light weight composites for improving thermal management** in order to maintain a high temperature gradient between the hot and cold sides of the TE device. Thermal management at both the hot and cold sides is just as important to device operation as high ZT. In the current approach to heat sinking, large metal plates with fins are used. These are high-density materials, which are very heavy and require significant machining, lead to an increase in the cost of the overall TEPG device. Fluid is typically used as the coolant media, which presents additional engineering issues. And finally, significant mismatch in the coefficient of thermal expansion between the metal and the TEPG legs lead to degradation of the device. The optimal thermal management material should have high thermal conductivity, have a coefficient of thermal expansion that is closely matched to the surrounding materials, and have low mass-density. These attributes would help towards eliminating fluid-based cooling.

In collaboration with Dr. Singh of Penn State University, *we have recently developed novel thermal management materials, which meet these criteria.* We found that these novel composites have thermal conductivity approaching that of diamond. These new materials are a blend of copper with diamond and multi-walled carbon nanotubes (CNT). The material can be tailored to match the coefficient of thermal expansion of the module substrate/package materials, and the thermal conductivity can be engineered by adjusting the volume fraction of the diamond/CNT. Thus, the materials and compositions are customizable for specific needs. The material is produced by powder metallurgy using a one-step approach, which leads to significant cost savings in the end product. Therefore, along with the improvement in the thermal conductivity, this material is lightweight, cost effective and robust. During this Phase I program we further extended the thermal management work by using light weight Al, pyrolitic graphite flakes and carbon nanotube composites, which is a very promising approach and is described in detail later in the report.

4. Results and Discussion

A summary of the work carried out during Phase I is as follows:

1) Materials synthesis and XRD
2) Sintering and XRD
3) Preparation of n- and p-type legs
4) Electrical measurements on legs
5) Device fabrication and characterization
6) Investigation of Thermal Management

4.1 Materials Synthesis and XRD

Magnesium silicide (Mg_2Si) is a narrow band gap semiconductor (Eg ~ 0.3–0.6 eV), with low density (below 2 g/cm^3) and high melting temperature (1358 K) [26]. Mg_2Si and its alloys consist of anti-fluorite crystal structure with Si in the FCC (face centered cubic) sites and Mg in the tetrahedral positions. Based on the simulations by Zaitsev et al [24], it is believed that this type of TE material can attain greater ZT values because of high carrier mobility, large effective mass and comparatively low phonon scattering.

Therefore, in recent decades, Mg_2Si has attracted attention as a mid-to-high temperature range TE material; however, it also has been identified as very difficult to synthesize with good crystalline quality because of the dangerous process temperature required for the melt growth of Mg_2Si. The melting point of Mg_2Si is 1085°C, and thus ~1150°C or slightly higher temperature is needed obtain good crystalline quality. However, this process temperature is beyond the "boiling temperature (1090°C)" of Mg. Furthermore, high reactivity of Mg in molten and vapor phase at these temperatures makes synthesis from molten state difficult and causes problems by sticking to the crucible material, often rupturing the crucible resulting in material contamination. In the past various crucible materials were tried [25] for synthesis of Mg_2Si but only boron nitride crucibles were found to work. For these reasons, the conditions for growth of high-quality single crystals and the doping control needed to establish *p*-type and *n*-type conductivities have

not been well-established as of yet, despite the fact that Mg_2Si is the only stoichiometric silicide in the Mg-Si phase diagram (Figure 1).

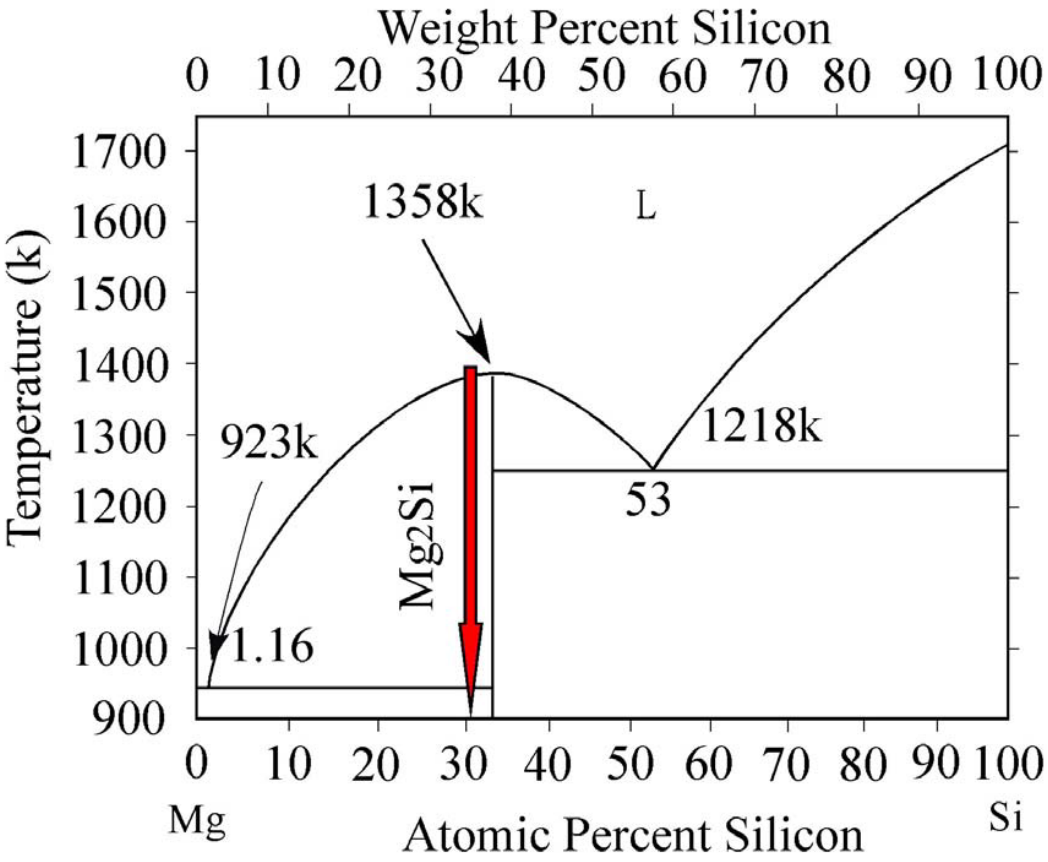

Figure 1. Mg-Si phase diagram [25].

Recently, the advent of nano-processing techniques has led to solid-state synthesis via mechanical attrition/ball milling as an attractive method to synthesize compounds which are difficult to react and synthesize from the molten state. But the ductile characteristics of Mg and reactivity of Mg with oxygen still make this synthesis process a challenge. Some reports mention contamination due to grinding media during ball milling [26]. However there are reports of successful Mg_2Si synthesis in inert or controlled environment.

During Phase I we designed a novel method to synthesize both Mg_2Si and $MnSi_{(2-x)}$ by directly reacting the starting elements in pyrolytic Boron Nitride (pBN) ampoules/crucibles, under nitrogen environment. This method of synthesis is simple, rapid and low cost. We first synthesized these silicide materials and then ball milled them, in an argon environment, to produce nano-powders. Using these powders and FAST/SPS we produced bulk nanostructured magnesium and manganese silicides. The details of synthesis work and results are presented as follows:

.

Synthesis of Bulk Mg_2Si and $MnSi_{(2-x)}$:

The silicides were synthesized from elemental magnesium and silicon (with Sb as a dopant in most syntheses) and manganese and silicon respectively. 6N silicon (Virginia Semiconductors was ground and sifted (mesh 80) to produce powder reacting with Mg and Mn, respectively. Magnesium was in the form of small pieces (up to ~ 3 mm in size), while Mn was as a coarse powder (grains ~0.5 mm and less). For the initial tests magnesium grit >99.0% (Sigma-Aldrich) was used. After the synthesis procedure had been established, we used high purity Mg and Mn obtained by repeated sublimation of low purity (~99 to 99.9%) starting metals under dynamic vacuum. Brimrose has optimized these purification processes for both Mg and Mn.

During the initial attempts to synthesize Mg_2Si, stoichiometric amounts of Mg and coarsely ground Si (a total of about 35g) were mixed together and loaded into a pyrolytic Boron Nitride (pBN) crucible which was then sealed under vacuum in graphitized silica ampoule. As a safety precaution, the ampoule was placed in a thick-walled metal tubing (in case of a rupture caused by self-accelerated progress of the highly exothermic synthesis reaction). The tubing with the ampoule was placed in a vertical tubular furnace and its temperature was gradually raised up to about 1150°C over a period of 75 hours, kept there for another 24 hours, then translated at 1 mm/hr thru the maximum temperature, down the temperature gradient for 160hr, and finally cooled down to room temperature (RT) in the furnace. The synthesis showed that the rate of heating the ampoule was sufficiently slow to prevent a potential explosion (for our amount of the reagents and type of confinement). However, there were clear signs of reaction between the magnesium and pBN, and Mg and silica (by Mg vapors escaping the pBN crucible). Also, the reaction was apparently incomplete, due to relatively large grains of silicon and temperature being well below the silicon melting point.

To mitigate the above problems, our following attempts of synthesis were conducted in a specially fabricated pyrolitic graphite crucible with a lid, and the ampoule was backfilled with nitrogen (0.2 atm at RT, about 1 atm at the maximum temperature during synthesis). Also, silicon was finely ground and sifted (mesh 80). The pyrolitic graphite crucible was to prevent any reaction with the crucible materials, while the closed configuration of the crucible and a presence of nitrogen reduced diffusion of magnesium vapors out of the crucible, thus reducing its reaction with unprotected parts of the silica envelope. Temperature timeline was similar to that used in the first synthesis. Those conditions turned out to be insufficient to prevent escape of larger amounts of Mg vapors from the crucible and its reaction with silica envelope. As a result, the damage to the ampoule leads to its cracking during cool-down. Another attempt under similar conditions leads to a breakage of the ampoule at low temperature due, again, to its etching by Mg vapors.

To reduce the time of the reaction (and, thus, the time of the Mg vapors etching the silica ampoule), we attempted to synthesize the material in a short time period of a few hours. That attempt lead to an explosion, apparently due to the self-acceleration of the reaction rate caused by a fast increase of the temperature by the release of latent heat.

The above unsuccessful series/ of tests lead us to a new design of the synthesis assembly shown in Figure 2.

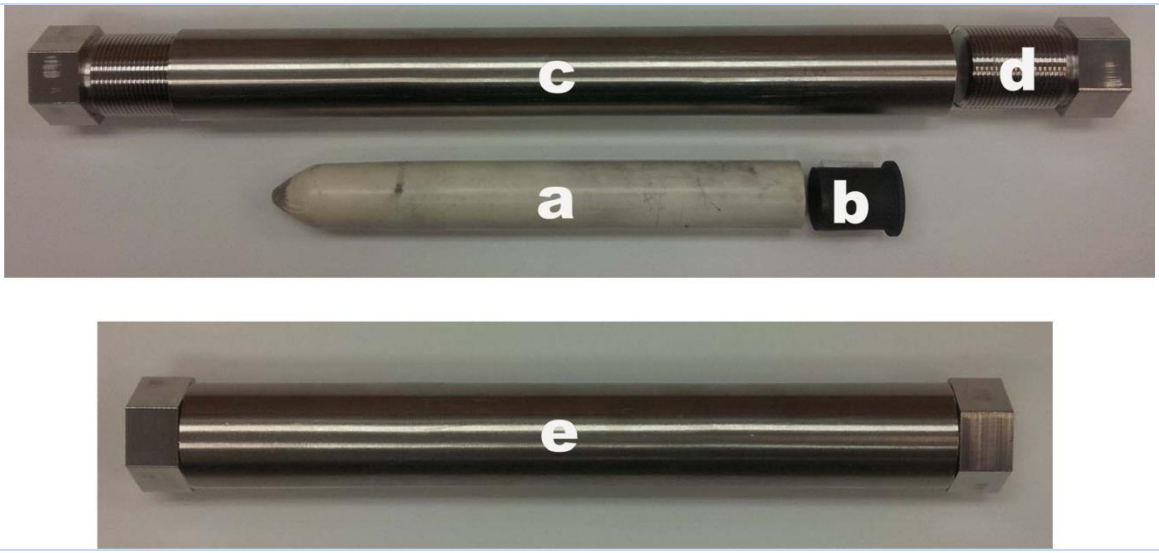

Figure 2. Syntheses assembly and its elements.

The material (the appropriate mix of elements) is placed in a pBN crucible (a), which has a tight fit graphite plug (b). The loaded and plugged crucible is put into a thick-walled metal tube container (c) closed at each end with a long bolt (d); the elongated bolt and its fine thread is to reduce the rate of loss of metal vapors out of the container. The whole assembly (e) is put together in a glove box. First the glove box is evacuated when the metal tube containing pBN are open. Then glove box is purged /back filled with nitrogen and pre weighted amounts of Mg and Si are filled in the pBN tube. The pBN tube then is plugged with the tight fit graphite plug. The pBN tube with the graphite plug is inserted into the metal tube and bolted tightly on both sides. Then the whole assembly is taken out of the glove box and immediately inserted in the furnace. The temperature of the crucible is quickly raised to 800°C, and then in about 1hr to 1120-1150 °C where it stays for 1-4 hours, after which the furnace is turned off. Loading the materials into the crucible in a glove box and backfilling it with Nitrogen, as well as a tight (albeit not complete) sealing of the reaction chamber minimizes the loss of Magnesium from the reactor, at the same time practically preventing oxidation of the materials inside the crucible. A strong metal envelope enables a short time of synthesis without a danger of an explosion from an overpressure during a fast acceleration of the reaction.

This procedure was used successfully for the remaining syntheses of the silicides. They included one synthesis of $MnSi_2$, two syntheses of $MnSi_{1.7}$, one synthesis of undoped Mg_2Si, two syntheses of Mg_2Si doped with 4% Sb, one process of re-melting commercial Mg_2Si chunks (doped with 0.5% Sb, Yasunaga, Japan), and one process of remelting our own synthesized and cleaned Mg_2Si.

The materials after synthesis are composed of a compact slug and loose powder and spongy pieces, as shown in Figure 3 for Mg_2Si and $MnSi_{1.7}$.

Mg_2Si	$MnSi_{1.7}$

Figure 3. The products of syntheses.

The bottom picture of MnSi product in Figure 3 is shown after cleaning the ingot in Methanol. The loose powder consists primarily of silica, apparently coming from oxidized surface of Si powder. Remelting of a cleaned ingot of our synthesized silicide yields a product devoid of any loose residues.

Figure 4 shows a photograph of remelted Mg_2Si and Figure 5 shows the photograph of remelted $MnSi_{1.74}$. It can be seen that they look quite clean.

In one of our processes we remelted commercial Magnesium Silicide from Yasunaga, Japan. It produced a compact ingot without any powder residues. However, when the ingot was cleaned in Methanol to remove some pBN residue from the crucible wall (Figure 6), an exothermic reaction occurred and the entire ingot was destroyed. We believe that this reaction was most likely the result of a large excess of Magnesium present in the starting material.

Figure 4. Remelted Mg_2Si Ingot.

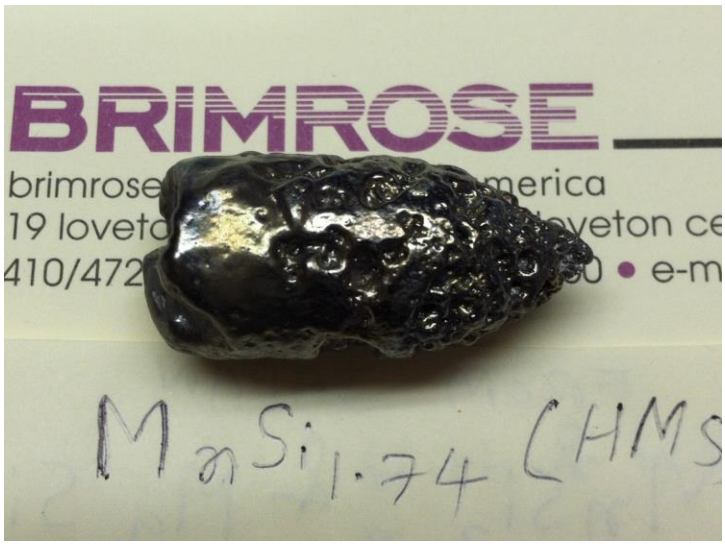

Figure 5. Remelted $MnSi_{(1.74)}$ Ingot.

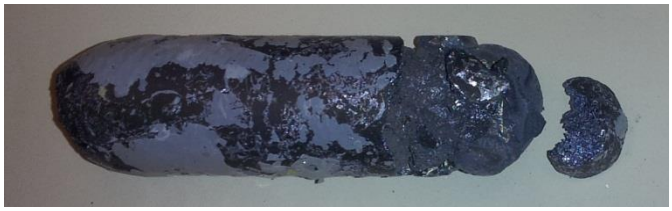

Figure 6. Ingot of remelted Magnesium Silicide chunks from Yasanuga, Japan.

A fast synthesis of the silicides could be accomplished in a completely sealed, strong metal container (backfilled with inert gas). However, such a solution would require welding the container and cutting it open for every synthesis, which would add material and labor costs to the process. It should be noted that during the synthesis the entire reaction assembly needs to be at the same temperature; if the crucible is placed in a metal container/tube with parts of the container at (considerably) lower temperature, such configuration would facilitate the loss of magnesium thru its deposition in the cooler parts of the system.

In our technique, loading the materials into the crucible in a glove box, putting it into the pressure metal container, and back filling the assembly with Nitrogen, as well as a tight (albeit not complete) sealing of the reaction chamber can minimize the loss of magnesium from the reactor, at the same time practically preventing oxidation of the materials inside the crucible. A strong metal envelope allows for a short time of synthesis (until completion) without a danger of an explosion from the overpressure during a fast acceleration of the reaction rate.

The essential features of our synthesis technique are:

- inert gas atmosphere,
- pyrolitic boron nitride crucible with its well fitted graphite plug,
- mechanically strong reusable, and tightly sealed outer container (steel).

The importance of these features is as follows:

A short time of the synthesis is necessary to minimize the time during which magnesium, which has a relatively high vapor pressure at elevated temperatures, can escape from the crucible and change the composition of the final product in a hard to control way. A fast synthesis can be accomplished by a fast increase in the temperature of the reaction mixture. The reaction is exothermic, and its fast progress easily gets accelerated leading to a sudden increase in the temperature and, thus, to high pressure of magnesium vapors. The steel outer envelope can withstand a substantial pressure developed in the system during fast progress of the reaction and prevent explosion/disintegration of the system at that stage of the synthesis.

Also, because Mg is a reactive species, when it escapes from the crucible it not only changes the composition of the final product, it can also react with some other parts of the system. The critical factor is the rate of transport of Mg out of the crucible. When the pressure inside the system (semi-closed system in our case) is the same as that outside, the mass transfer of gas species occurs by diffusion, which is a relatively slow process. When there is a difference in total pressures between two locations (here: inside and outside of the crucible and inside and outside the container) the mass flow is viscous, a fast mass transport process. In either case, the amount of materials transferred depends on the channels of transport, i.e. their lengths and cross-sections. To minimize the amount of material transported, the channels should be long and their cross-sections small. In our case, there are two constrictions:

The first one is between the pBN crucible opening and the graphite plug (element b in Figure 2). With the snug fit of the crucible and plug, the opening between the two is being formed practically only when the pressure inside the crucible exceeds the one outside. When that happens, the crucible expands a little allowing for the inside and outside pressure to equalize, and then the slit gets tiny again (the axial displacement of the plug is prevented by a close match of the crucible-plug assembly length and the inner distance between the bolts inside the steel container). When the pressure inside and outside the crucible is equal, the material exchange between those sections can occur only thru diffusion. Since the plug is well matched to the crucible opening, that exchange is very small, practically negligible.

The second constriction is between the metal container and the outside, and is accomplished by long bolts with fine pitch which close the container at each end. Once again, when the temperature of the assembly increases and the pressure inside goes up (initially just by thermal expansion of Nitrogen in the system), the gas attempts to escape thru the space left between the bolts and tube threads and the bolts head. Since the space is very tight, the loss of gas is very small. Moreover, until the pressure of Magnesium is low, the gas escaping (both from the crucible and the container itself) consists only of Nitrogen. Only when the pressure of Magnesium becomes comparable to that of Nitrogen, a substantial fraction of the escaping material may be Magnesium vapors. Nitrogen plays a role of a protecting blanket of gas, so it is primarily Nitrogen which is being pushed out first. Since the rate of loss (thru the constricted areas) is very low, and the period during which the pressure of Magnesium vapors is high is short, the amount of Magnesium that has a chance to escape from the crucible is low. Moreover, once the magnesium starts to react with silicon, the magnesium gets enriched in Si which reduces the equilibrium vapor pressure over the material. And, once the reaction is complete, which

apparently occurs quickly under our synthesis conditions, the pressure of magnesium vapors becomes low and no substantial loss of Mg from the system may occur.

Once the pressures inside and outside the container equilibrate, the only process that may affect the sample is its oxidation by air oxygen penetrating into the crucible. Since such a transport is then possible by diffusion only, and there exists Nitrogen which slows diffusion of other species, its rate is very slow and, under the actual geometry of our system and a short time of that period, is negligible.

The last stage of the process is that of cooling the assembly down. If during the high pressure period of the synthesis the container and outside pressures become equal, cooling down will reduce the pressure inside the container creating a "sucking" action which will accelerate influx of the outside air into the system with a possible oxidation of the sample (when at high temperatures). However, the oxidation would occur on the surface of the already solidified synthesized product becasue the inside of the crucible is well sealed off by the plug, and the cool-down occurs relatively fast. Also, later fine-tuning improvements to the technique led to the conclusion that oxidation of material during the process can practically be avoided; while the initially achieved products (Figure 3) included some amounts of a light powder (oxides), the last ingots (Figure 7) were essentially free of them. The technique works also for manganese silicides, which are even less technologically challenging than those with magnesium due to much lower equilibrium pressure of Mn under the experimental conditions.

Figure 7. Optimized as Synthesis of Mg_2Si:Sb ingot.

Our technique of the synthesis of magnesium and manganese silicide solves, in an economic way, the problems of (1) high pressure developed during the synthesis, (2) high reactivity of Mg and Mn and (3) it minimizes the loss of magnesium from the reaction mixture or its oxidation by the air. The developed technique offers:

- a fast process (a few hours, which may probably be reduced to 3hr),
- a reusable confining assembly,
- a good control/retaining of the composition/stoichiometry of the starting mixture.

We plan to scale up the technique for production of thermoelectric silicides during the Phase II program.

4.2 Sintering of Nanopowders

In conventional hot pressing techniques, the powder container is typically heated by radiation from the enclosing furnace through external heating elements and the resulting heating rate is slow. Field assisted sintering technology is similar to traditional hot-pressing, but in this case the powder compact is heated by a high-intensity, low-voltage pulsed DC electric current flowing directly through the sample (if electrically conducting) and through a die, typically made out of graphite. As a consequence of FAST during the sintering process, the powder sample can experience heating rates as high as 1000^0C per minute. This facilitates efficient consolidation and inhibits grain growth.

In FAST the temperature required to attain 95% of the theoretical density decreases exponentially with pressure. As shown in Figure 8, in case of nano-crystalline zirconia pressure as high as 1 GPa maintained during FAST can cause full densification in five minutes and at a temperature that is several hundred degrees below the conventional sintering temperature. The decrease in sintering temperature and duration causes marked decrease in grain growth. Thus, high pressure FAST is an ideal technique to process transparent ceramics and thermoelectric materials where grain structure is very critical.

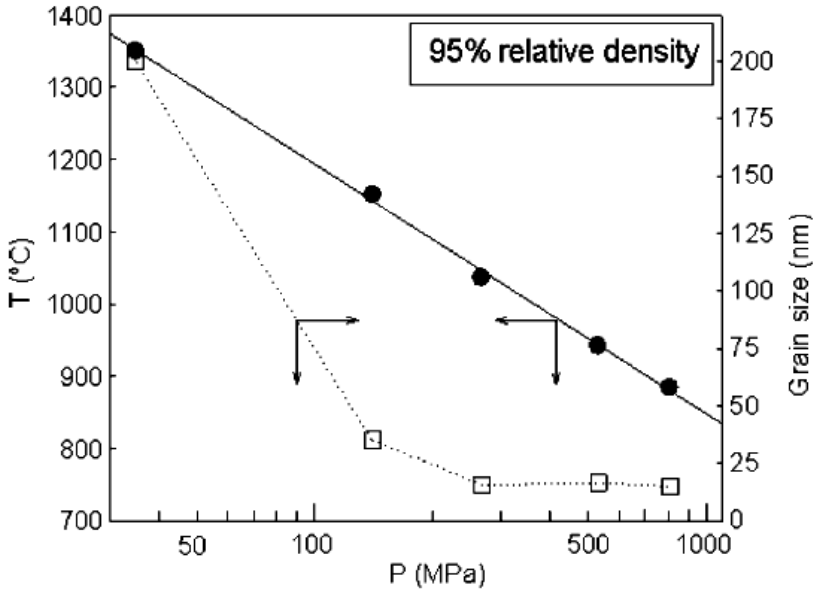

Figure 8: Relationship between hold temperature, applied pressure and resulting grain size in Field Assisted Sintering Technology [27].

Major SPS sintering parameters are heating and cooling rate, dwell time and applied pressure. For SPS sintering of $MnSi_{1.75}$, the sintering temperature is generally believed to be around 850°C [28,29], and for Mg_2Si, sintering temperature has been reported to be between 650-850°C [30]. The optimum sintering temperature for a specific batch of powder is determined by the morphology and size of the powder, sintering time, and the applied pressure.

Table 1 shows a summary of the bulk nanostructured samples of Mg_2Si and MnSi. prepared by FAST.

For our MnSi powder, we compared three sintering temperatures: 700°C, 800°C and 900°C at 50MPa with sintering time between 5-20 minutes, and the obtained samples were evaluated based on their electric conductivity and density. We concluded that a condition of 900°C for 20 minutes at 50MPa gives the best performing samples for $MnSi_{1.75}$.

For our Mg_2Si samples, we compared several sintering temperatures ranging from 750-1000°C and discovered that the sintering behavior of Mg_2Si depends even more so on its size/ morphology than it does for MnSi. Micron grained Mg_2Si stock powder (hand ground with a mortar and pestle) will not sinter even at 900°C, and only start to sinter at temperature above 950 °C. Meanwhile nano-grained Mg_2Si (ball milled to nanometer sizes) can easily sinter at 750 °C. Therefore, *nano-grinding is a crucial step for sintering Mg_2Si powders.* Nano-grinding can also be applied to MnSi powder to reduce sintering temperature. Our latest sintering condition for nano-ground Mg_2Si is: 750°C/50MPa/10min. This sintering condition produced Mg_2Si with excellent electrical conductivity (details on these measurements are later in this report. However, samples obtained often develop cracks.

In order to prevent crack formation in sintered Mg_2Si samples, we also investigated the effect of metallic binders on the sintering behavior of Mg_2Si powder [31]. Two metals, copper (Cu) and nickel (Ni), were chosen as binders at 5wt%. The Cu doped Mg_2Si powder was sintered at 800°C/50MPa/10min and the Ni doped Mg_2Si powder was sintered at 900°C/50MPa/10min. Both samples exhibit excellent mechanical and electric properties and this suggests that metallic binders could be used to improve the sintering of thermal electrical materials. However, the effect of these metallic binders on the thermal conductivity and thermoelectric performance needs to be evaluated in detail. This detailed study of the effect of these metallic binders will be carried out systematically in Phase II. However during Phase I we have used 4 wt.% of Ni as a binder for Sb doped Mg_2Si nano-powder, after the published work of Hayatsu et al. [31]. The material shows n-type behavior and respectable Seebeck coefficient as shown in device characterization section.

X-Ray Diffraction Measurements

The nano-powders and sintered bulk nanostructured samples were tested for their compositional homogeneity using X-ray diffraction (XRD) (Figures 9 to 14). Figure 9 shows the XRD of Sb doped Mg_2Si powder, Figure 10 is for sintered Sb doped Mg_2Si and Figure 11 is sintered Sb doped Mg_2Si with 5% nickel added as a binder. Figure 12 is the reference Mg_2Si XRD pattern showing variation of the pattern with stoichiometric change. The comparison clearly indicates that *our samples were stoichiometric Mg_2Si materials*. These samples were used for electrical characterization and device fabrication (details to follow). Figures 13 and 14 are x-ray diffraction measurements of Sb doped $MnSi_{(1.74)}$. Figure 13 is the sample prepared during this work, and Figure 14 is the reference XRD pattern.

Typical silicide samples prepared using FAST are shown in Figure 15(a) and 15(b).

Table 1. Table summarizing the bulk nanostructured samples prepared by FAST.

Brimrose Thermoelectric Materials -SPS								
Date	Run #	Powder Wt. (g)	Dia (mm)	Temp (°C)	Press (MPa)	Time (min)	Env.	Comments
10/2/13	2074	4.462	20	200	100	20	Argon	#1 MgSi2 30A12 nano used thick wall 20mm graphite die with steel punches and 60mm endpieces - material did NOT
10/2/13	2076	4.043	20	350	100	20	Argon	#1 MgSi2 30A12 nano used thick wall 20mm graphite die with steel punches and 60mm endpieces - sample OK recipe error - hold step set to 200C so temp dropped from 350C to 200C over 20
10/2/13	2078	5.26	20	350	100	20	Argon	#2 MgSi2 30A12 nano used thick wall 20mm graphite die with steel punches and 60mm endpieces - sample OK
10/2/13	2079	4.275	20	350	100	20	Argon	#1 MgSi2 undoped - sample OK
10/2/13	2080	4.569	20	350	100	20	Argon	#5 MgSi2 undoped nano - sample OK
10/3/13	2082	6.9995	20	350	100	20	Argon	MgSi2 Sb doped - sample OK
10/3/13	2083	7.0332	20	350	100	20	Argon	MgSi2 Sb doped 5% fullerene - sample OK
10/15/13	2099	12.7	20	800	45	5	Argon	MnSi2 - sample OK
10/15/13	2105	12.7	20	700	45	5	Argon	MnSi2 - sample OK
10/22/13	2115	6	20	750	50	2	Argon	Mg2Si-Sb PMS-12 batch #1 - processed twice - sample broke into
10/22/13	2116	6	20	800	50	5	Argon	Mg2Si-Sb PMS-12 batch #1 - processed twice - sample appeared OK but broke when removing foil
10/22/13	2117-2118	6	20	900	50	20	Argon	Mg2Si-Sb PMS-12 batch #1 - processed twice - TC2 broke during first run - replaced TC and started again - sample appeared OK but broke when removing foil
10/22/13	2119	6	20	1000	50	5	Argon	Mg2Si-Sb PMS-12 batch #2 - unprocessed - some melting around 975C to 1000C - sample OK
10/23/13	2120	6	20	920	50	20	Argon	Mg2Si-Sb PMS-12 batch #3 - unprocessed - some melting but less than run #2120 - sample OK
10/23/13	2121	13	20	900	50	5	Argon	P MnSi #7 - sample OK
10/23/13	2122	13	20	900	50	5	Argon	P MnSi #9 - sample OK
10/23/13	2123	6.3	20	850	50	10	Argon	Mg2Si-1 5% Cu(wgt.)(batch #1) - sample OK - slight melting out of some material
10/23/13	2124	6.3	20	850	50	10	Argon	Mg2Si-1 5% Ni(wgt.)(batch #1) - sample cracked
10/23/13	2125	13	20	900	50	20	Argon	9.8 gm P MnSi batch #7 3.2 gm P MnSi batch #9 sample OK
10/23/13	2126	6.3	20	800	50	10	Argon	Mg2Si-1 5% Cu(wgt.)(batch #1) - sample OK - slight melting out of some material
10/23/13	2127	6.3	20	900	50	10	Argon	Mg2Si-1 5% Ni(wgt.)(batch #1) - sample OK - slight melting out of some material
10/30/13	2137	4	20	750	50	10	Argon	Mg2Si - old sample and some melted pieces - ground and roller milled 24 hrs. - sample cracked

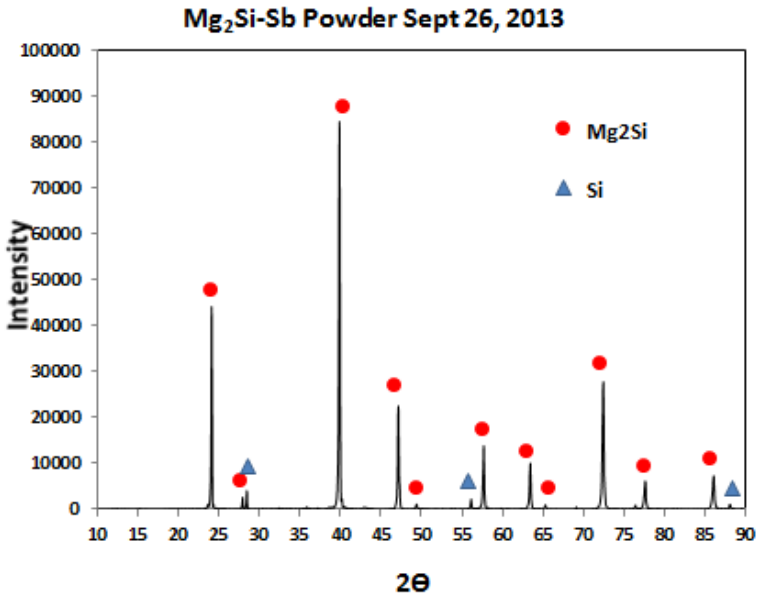

Figure 9. X-ray Diffraction pattern of Sb doped Mg_2Si nanopowder.

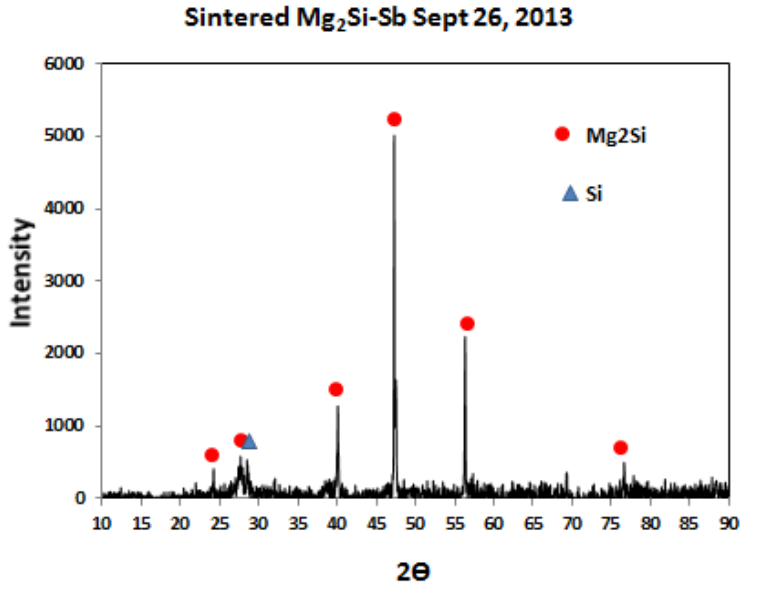

Figure 10. X-ray Diffraction pattern of sintered bulk nano-composite of Sb doped Mg_2Si.

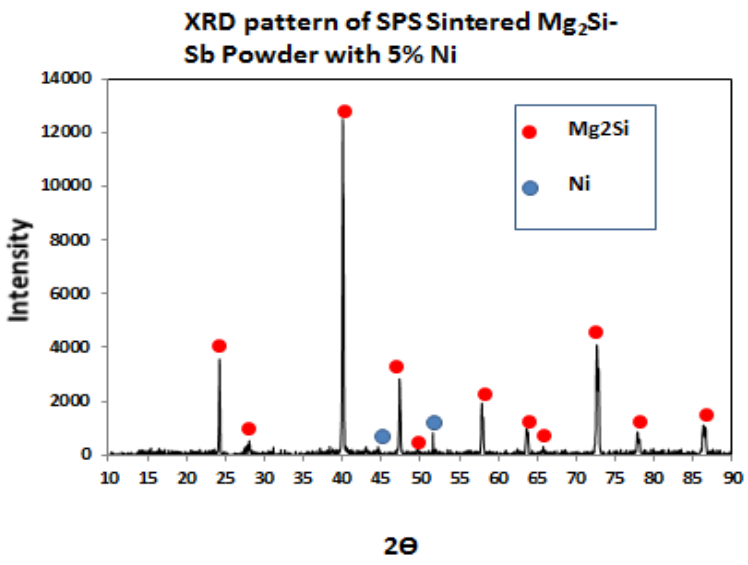

Figure 11. X-ray Diffraction pattern of sintered bulk nano-composites of Sb doped Mg_2Si with added nickel (Ni).

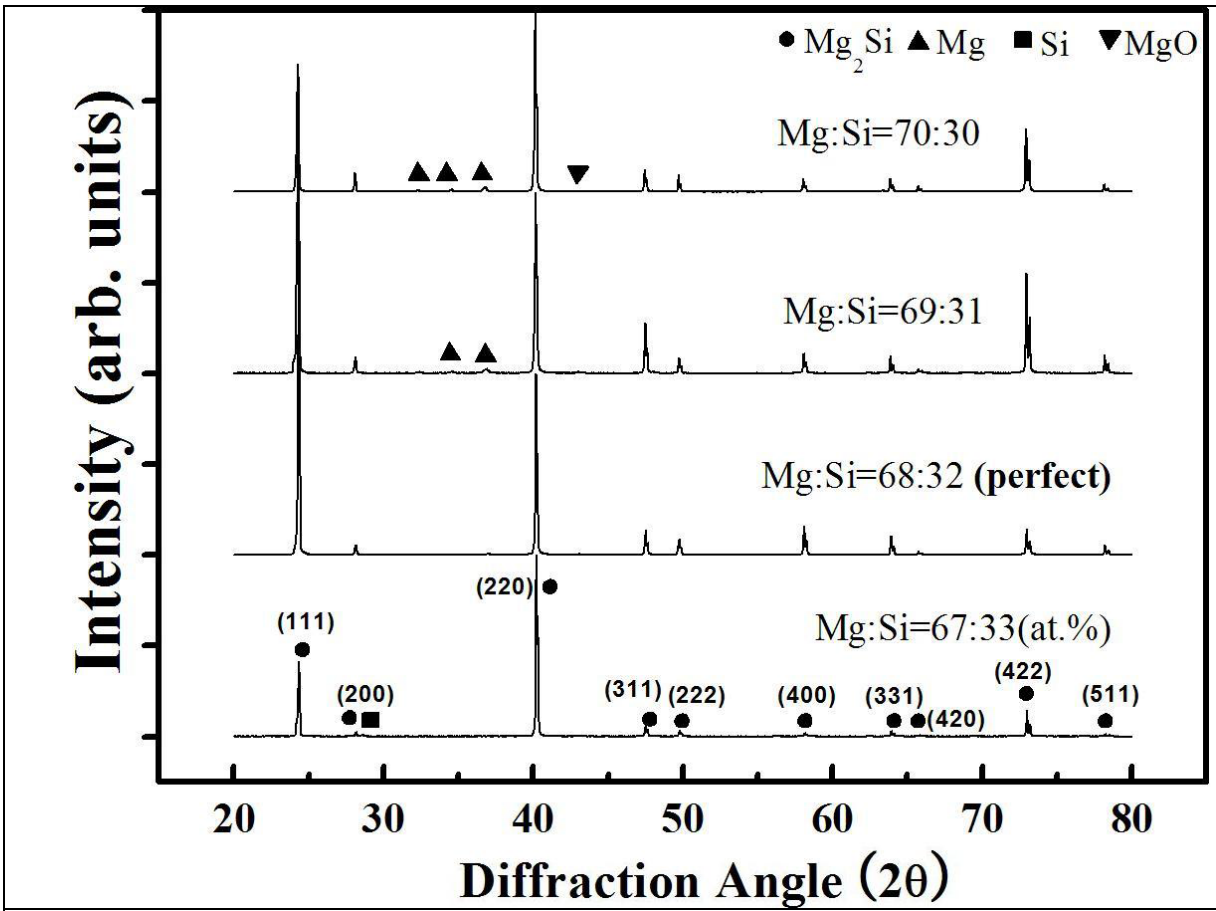

Figure 12. Reference x-ray diffraction pattern of Mg_2Si at various stoichiometry from Kim et al [32].

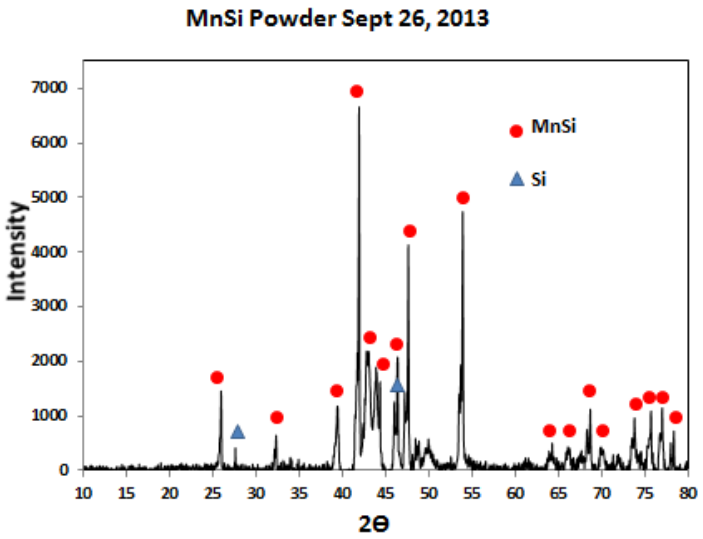

Figure 13. X-ray Diffraction pattern of MnSi nanopowder.

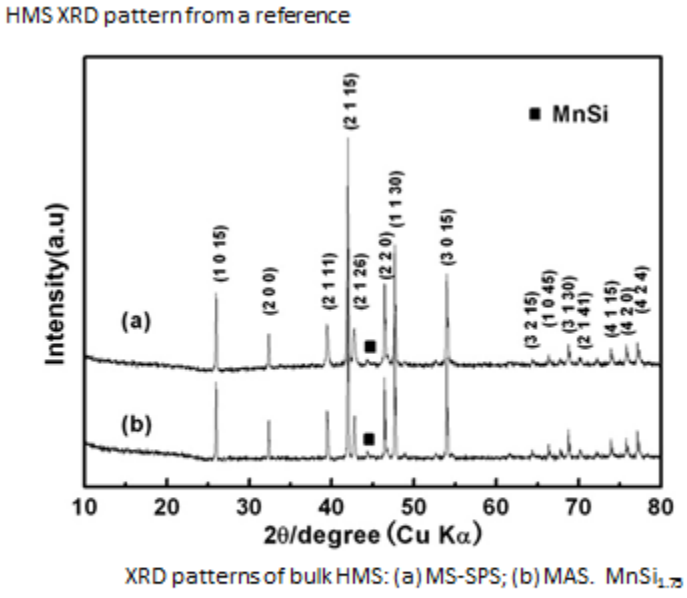

XRD patterns of bulk HMS: (a) MS-SPS; (b) MAS. $MnSi_{1.75}$

"Rapid synthesis of high thermoelectric performance higher manganese silicide with in-situ formed nano-phase of MnSi", Intermetallics 19 (2011) 404-408.

Figure 14. Reference x-ray diffraction pattern of MnSi at various stoichiometry [18].

a

b

Figure 15. Photograph of FAST sintered nanocomposites of Mg_2Si and MnSi produced during this work.

Optical Micrographs of Sintered Nanocomposites

We also optical micrograph photographs of the samples that we produced during the Phase I program as well as the samples that we purchased from Japan for comparison purposes. Figures 16 through 19 show the low and high magnification optical micrographs of the Japanese Mg_2Si and MnSi followed by the in-house produced material. The microgrpahs clearly show that our material are densely packed/sintered.

200x

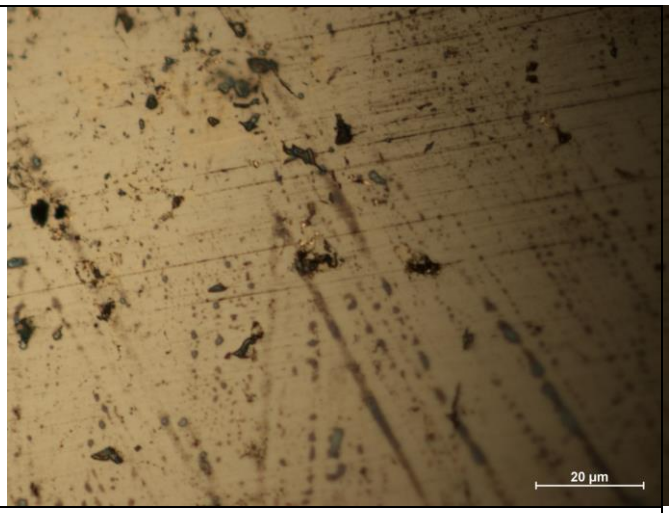

1000x

Figure 16. Optical micrographs of the Japanese Mg_2Si material at 200X and 1000X. This sample is nearly fully dense with scattered pores in 2-8 µm range.

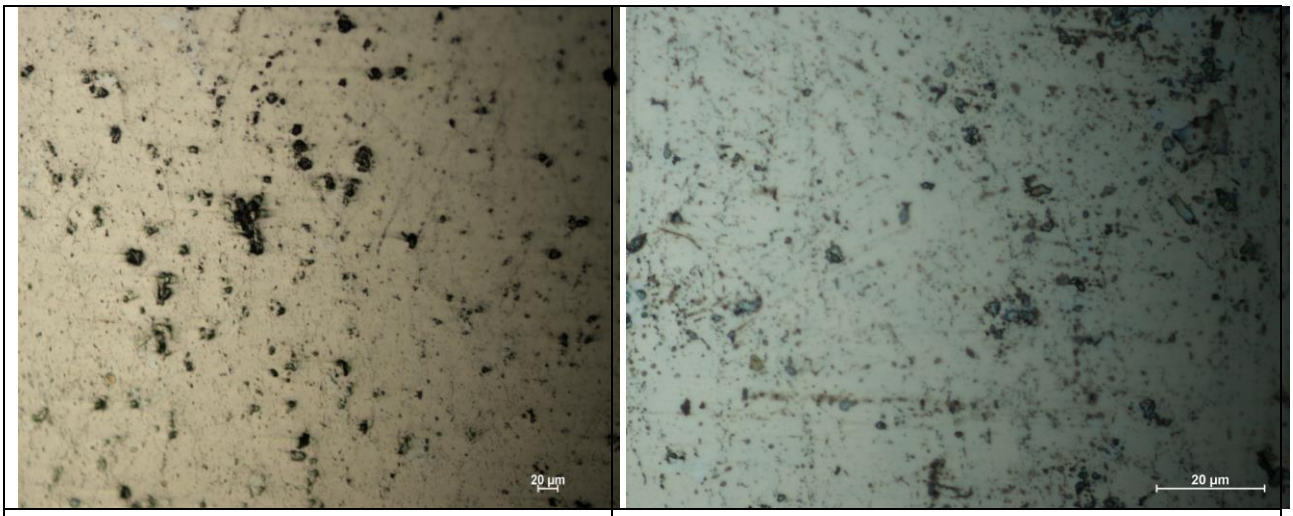

200x	1000x

Figure 17. Optical micrographs of Japanese MnSi at 200X and 1000X. This sample has pores in 1-5 µm range.

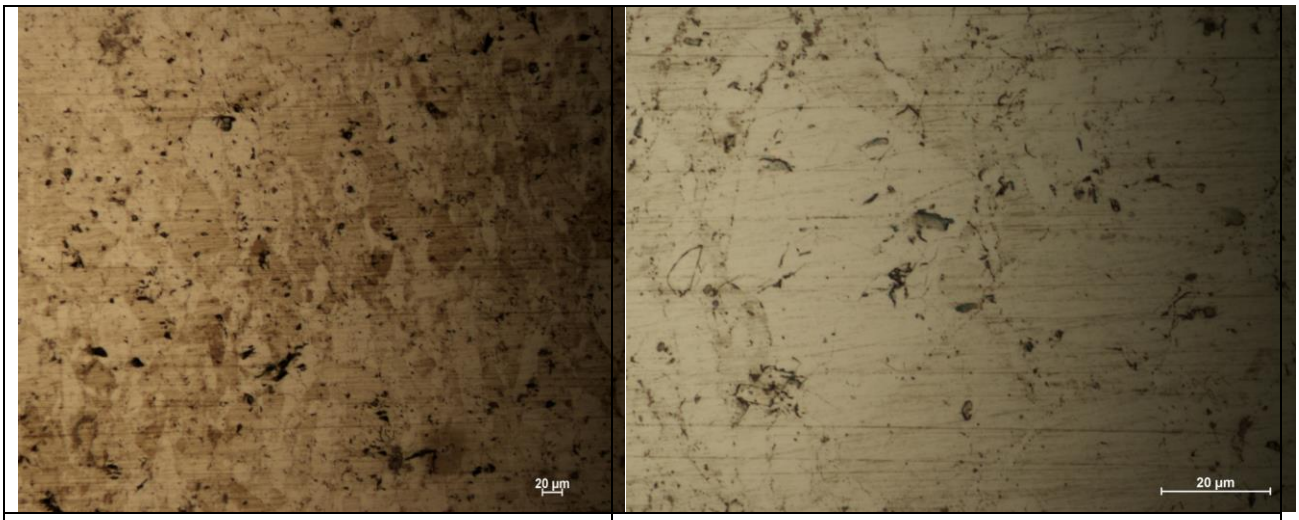

200x	1000x

Figure 18. Optical micrographs of Brimrose Mg_2Si at 200X and 1000X. This sample is almost fully dense with little porosity.

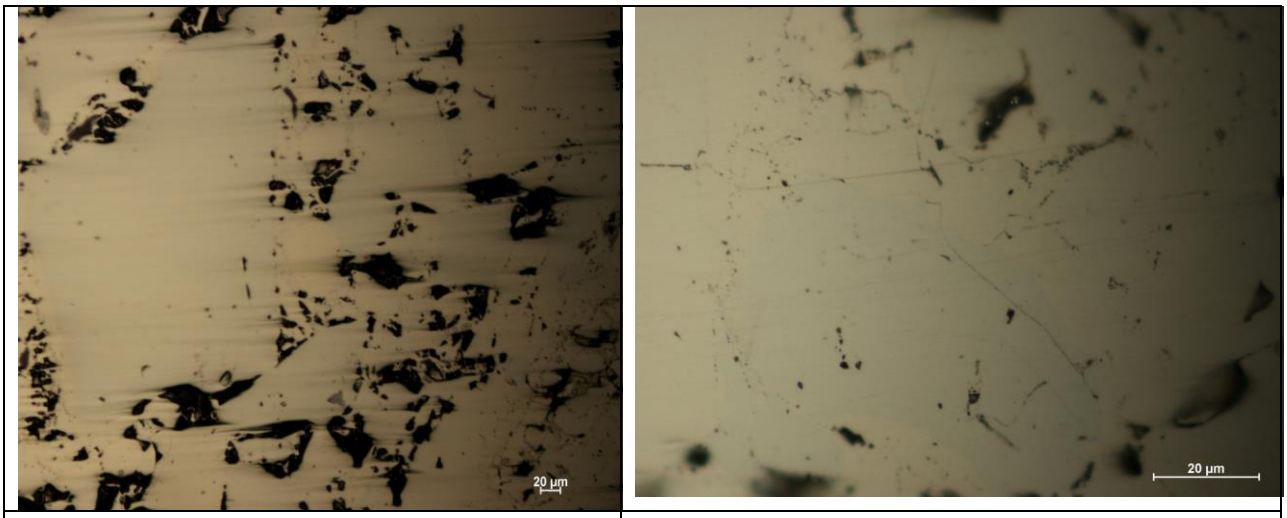

a b

Figure 19. Optical micrographs of Brimrose MnSi at 200X and 1000X. This nearly fully dense with isolated large pores (5-15 µm).

4.3 Preparation of N and P-Type Legs

Using the sintered n- and p-type silicides we prepared n- and p-type legs for fabricating Thermo Electric Power Generating (TEPG) devices. Leg dimensions were 3mm x 3mm x 6mm. Before cutting the legs we electrochemically deposited nickel layers on both sides of the sintered disks of the silicide materials. This was useful for putting high temperature ohmic contacts onto legs using a technique we developed earlier [23].

Prior to device fabrication, the following steps were performed:

1. Sintered Mg_2Si and $MnSi_{(1.75)}$ discs/pellets were ground and polished on both sides.
2. Nickel was electroplated on both sides of the sintered pellets,
3. N- and p-type legs with dimernsions 3x3x6 mm3 were mechanically cut,
4. Electrical resistance/resistivity measurements of TEPG legs

Electroplating of Nickel on Thermal Electrical Materials:

The electroplating of nickel on TE materials (sintered disks) followed the Watts process with nickel sulfate and nickel chloride as the main ingredients for the plating bath. The electroplating kit was purchased from Caswell Inc. Before plating, sample surfaces were ground flat and slightly polished, and degreased with thinner and acetone. The normal thickness of Ni coating for thermal electric contacts was 2 microns, and the coating thickness was adjusted by varying current density and/or plating time. For 2 micron Ni coating, our preferred current density and plating time were 1A dm^{-2} and 10 minutes, respectively. Figure 20 shows experimental setup for the nickel plating.

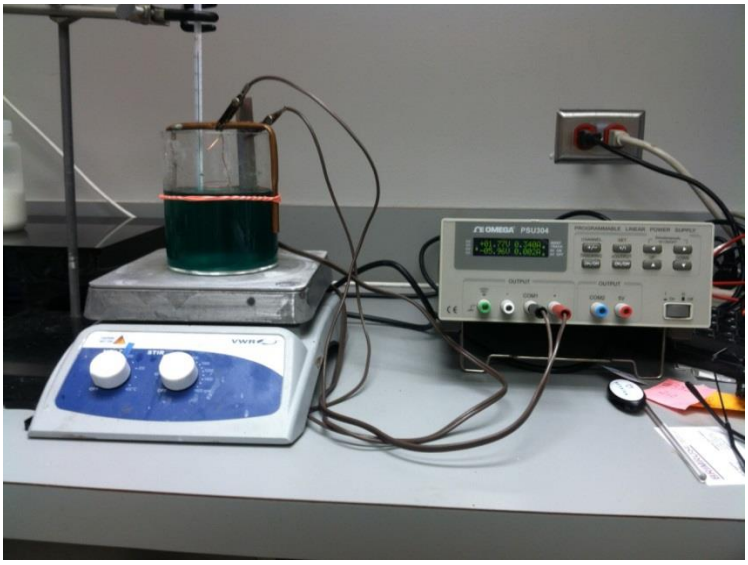

Figure 20. Experimental Setup for Nickel plating

Process of Nickel deposition was standardized and the thickness of the Nickel layers was determined by weighing the samples before and after nickel deposition, using a microbalance and pellet dimension measurements using calipers. Typical results are presented in Table 2. Figure 21 shows a photograph of typical sintered pellets before and after nickel deposition.

Table 2. Electrodeposition of Nickel: optimized deposition conditions.

Deposition Thickness (µm)	Weight per Unit Area (g dm^{-2})	Ampere Hours per Unit (Ah dm^{-2})	Time(min) to Obtain Deposit at Various Current Densities (A dm^{-2})				
			0.5	1	1.5	2	3
2	0.18	0.17	20	10	6.8	5.1	3.4
4	0.36	0.34	41	20	14	10	6.8
6	0.53	0.51	61	31	20	15	10
	0.71	0.68	82	41	27	20	13
10	0.89	0.81	100	51	34	26	17

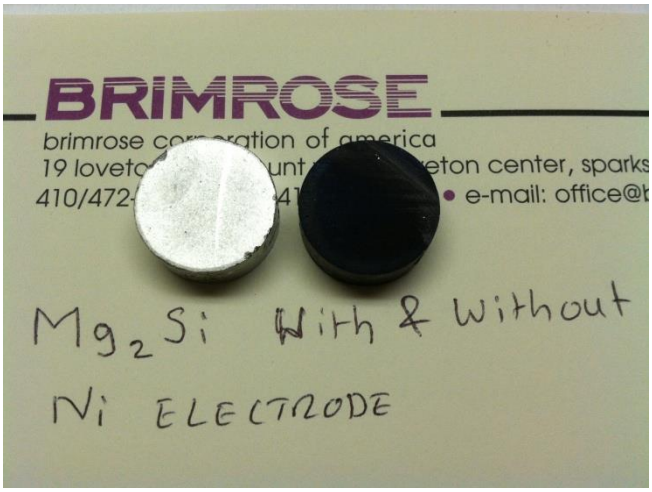

Figure 21. Photograph showing typical nickel plated sintered pallet.

Preparation of n-type (Mg_2Si:Sb) and p-type ($MnSi_{(1.75)}$) TEPG Legs:

Nickel coated pellets were blocked on a glass substrate using low temperature wax. Their surfaces were protected using lens tissues. Using thin diamond wheel 3mm X 3mm X 6mm size legs were cut. The sintered material was very dense and mechanically hard. After cutting the material was unblocked and the legs were cleaned using organic solvents. The cut pieces had sharp rectilinear edges. Figure 2 shows photographs of the n-type and p-type legs prepared in manner described above.

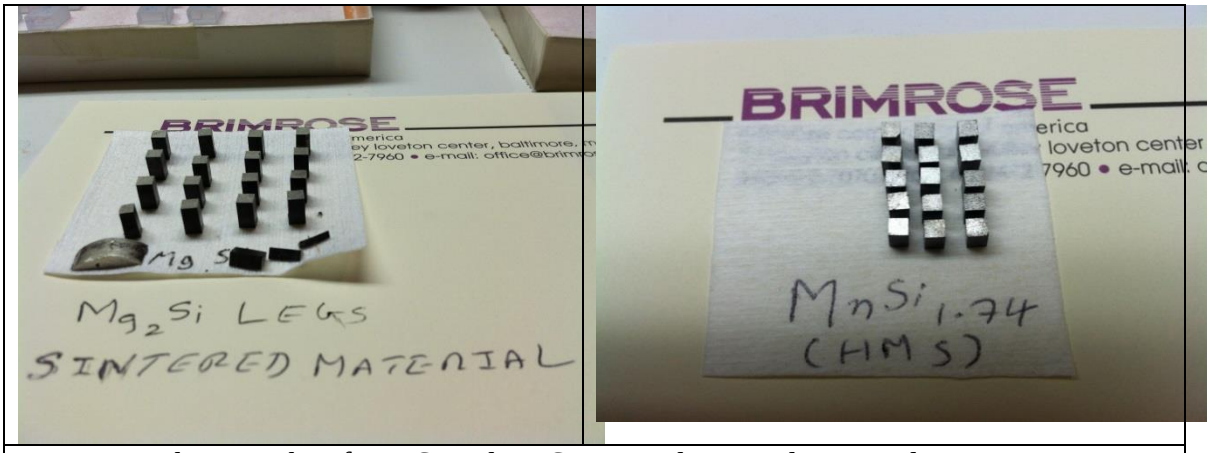

Figure 22. Photographs of Mg_2Si and MnSi sintered material cut into legs in preparation for fabrication of a thermoelectric device.

4.4 Electrical Measurements on Legs

Resistance measurements on TEPG legs were performed using a 4-point probe set up. We used a Hewlett Packard 34420A micro ohm meter which provided a built-in direct current 4-point resistance measurement. The sample holder consists of 2 copper bars, one of which is spring loaded, which are used both to hold the sample and pass current lengthwise through the sample. The measurement probes consisted of two pogo-pins space at 0.4cm and mounted in such a way as to allow 3-dimensional adjustment of the pins in order to center the pins on the sample. Testing was done in open air under room temperature. Figure 23 shows a photograph of resistivity measurement setup and a close-up of the sample holder. Resistivity measurement results are presented in Tables 3 and 4.

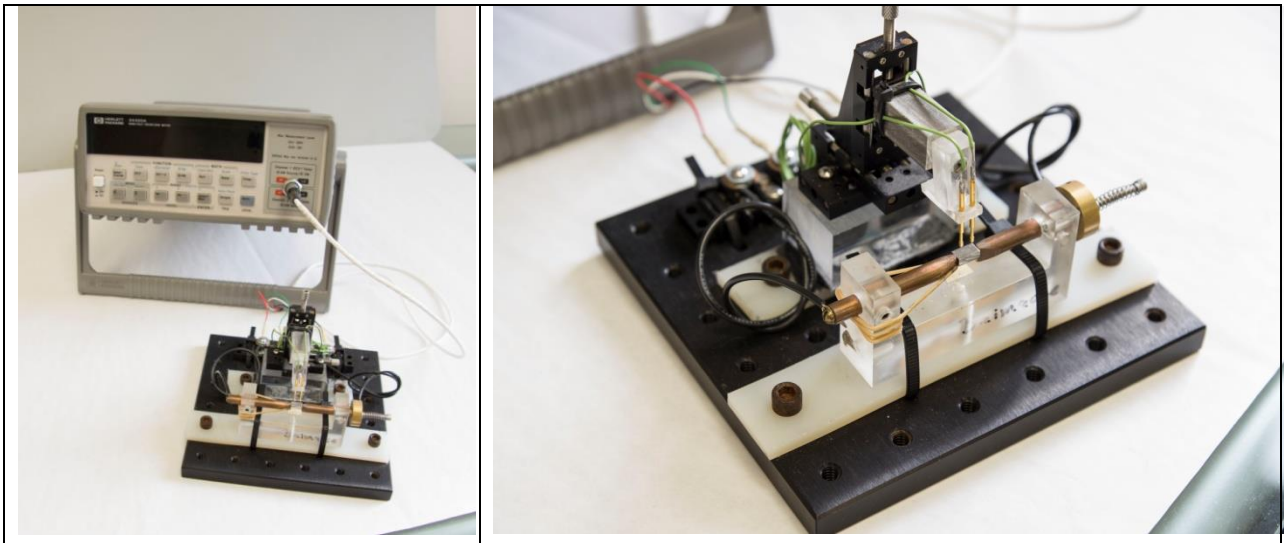

Figure 23. Photograph of resistivity measurement setup and a close-up of the sample holder.

Table 3. Resistance and Resistivity measurements for Mg_2Si.						
Mg_2Si						
#	l (cm)	w1 (cm)	w2 (cm)	mΩ	A (cm^2)	mΩcm
1	0.6	0.329	0.333	1.7	0.109557	0.465617
2	0.603	0.33	0.336	1.4	0.11088	0.38808
3	0.602	0.325	0.332	1.7	0.1079	0.458575
4	0.6	0.331	0.333	1.6	0.110223	0.440892
5	0.6	0.333	0.322	2.3	0.107226	0.61655
6	0.605	0.324	0.325	1.6	0.1053	0.4212
7	0.602	0.335	0.335	1.8	0.112225	0.505013
8	0.602	0.323	0.335	1.5	0.108205	0.405769
9	0.6	0.331	0.329	2	0.108899	0.544495
10	0.602	0.328	0.335	1.6	0.10988	0.43952
11	0.601	0.329	0.329	1.5	0.108241	0.405904
12	0.603	0.293	0.331	2.1	0.096983	0.509161
13	0.601	0.325	0.33	1.5	0.10725	0.402188
14	0.607	0.324	0.336	1.5	0.108864	0.40824
15	0.603	0.332	0.334	1.7	0.110888	0.471274
16	0.601	0.329	0.323	1.7	0.106267	0.451635

Table 4. Resistance and Resistivity measurements for MnSi.						
MnSi						
#	l (cm)	w1 (cm)	w2 (cm)	mΩ	A (cm^2)	mΩcm
1	0.603	0.326	0.335	5.4	0.10921	1.474335
2	0.604	0.333	0.33	7.7	0.10989	2.115383
3	0.604	0.326	0.323	5.6	0.105298	1.474172
4	0.602	0.331	0.323	7	0.106913	1.870978
5	0.603	0.335	0.329	6.1	0.110215	1.680779
6	0.6	0.331	0.329	7.1	0.108899	1.932957
7	0.606	0.333	0.325	6.2	0.108225	1.677488
8	0.601	0.329	0.328	6	0.107912	1.61868
9	0.601	0.326	0.329	6.6	0.107254	1.769691
10	0.604	0.334	0.331	6.3	0.110554	1.741226
11	0.607	0.333	0.329	6.4	0.109557	1.752912
12	0.604	0.324	0.329	6.8	0.106596	1.812132
13	0.605	0.331	0.323	6	0.106913	1.603695
14	0.602	0.334	0.331	5.6	0.110554	1.547756
15	0.605	0.334	0.328	6.2	0.109552	1.698056

4.5 Device Fabrication and Characterization

Device Fabrication

During this Phase I work we fabricated several single thermoelectric devices consisting of one n-leg and one p-leg, and a few 4 element devices consisting of 2-n type and 2p-type legs. We used nickel plated copper plates and selected low resistivity n-type Sb doped Mg_2Si legs and p-type $MnSi_{(1.75)}$ legs. These legs were prepared from FAST sintered bulk nanostructured material as described earlier. At the hot end of the device we connected/bonded n- and p-type legs using a nickel plated copper plate about 1 mm thick and 4 mm X 8 mm size. At the cooler end both n-type and p-type legs were bonded on the same size plates in an open circuit configuration.

The bonding process and bonding material that can provide ohmic contact from room temperature to the operating temperature is a very important part of successful device fabrication and operation with optimal efficiency. In silicide thermoelectric devices brazing is used for bonding of contact metals with n- and p-type legs. Typically nickel is used as the electrode material. In the brazing approach, a mixture of metals at the eutectic composition is applied between the two members to be joined. The metals are chemically aggressive and the composition of the active components of an electrical element (e.g., the thermoelectric materials) can be significantly degraded by chemical interaction and interdiffusion with the braze. Voids can form as a result of chemical interdiffusion between the components and the braze, and embrittled layers with poor mechanical properties can result. To successfully pursue this brazing approach, usually a more complicated, multi-layer solution composed of adhesion layers, diffusion barriers, and fluxes for the braze is utilized.

Magnesium silicide (Mg_2Si) is a promising advanced thermoelectric material operating in the temperature range from 600 to 900 K. However, electrode materials that exhibit stability at these operating temperatures have not yet been identified for n-type Mg_2Si. Although silver brazing (Ag-Cu-Zn alloy) is widely used as a contact electrode to TE materials for practical operation temperatures < ~1000 K, the contact resistance to Mg_2Si is not sufficiently low and the brazing process temperature is rather high. The electrical and thermoelectrical properties of n-type Mg_2Si with Ni have been studied using a monobloc sintering method, which provides simultaneous formation of metal electrodes during sintering of Mg_2Si [34]. Ni exhibited a stable boundary between the Mg_2Si and Ni layers, and its inter-layer adhesion properties were adequate at an elevated temperature of up to 900 K.

We attempted to develop an alternative method of developing high temperature ohmic contact using indium-nickel alloys. As we will see later, during this work we could bond TEPG legs using indium-nickel system and successfully fabricated a working TEPG device. However, the device resistance was very high, and despite the material having very good TE properties, we could not achieve high device efficiency. We plan to work on further development and optimizing the high temperature, low resistance contacts using indium-nickel alloy system.

In our fabrication process we sandwiched, thin (about 50 micron) indium-nickel-indium films, between nickel coated copper plates and nickel coated TEPG legs, in device configuration in a specially designed jig. This jig was transferred inside the vacuum chamber and placed between temperature controlled 250 watt flat heaters. After evacuating the chamber, the temperature of

both heaters was increased to 300^{o} C in 30 minutes and then to 600^{o}C in another 30 minutes. The assembly was kept at this temperature for 30 minutes and the power of both heaters was turned off. Upon cooling to room temperature the jig was removed from the vacuum chamber and the assembled device was removed.

Figure 24 shows the jig assembly in the vacuum chamber, and Figure 24 shows the device fabricated as described above.

Figure 24: Device Fabrication Setup

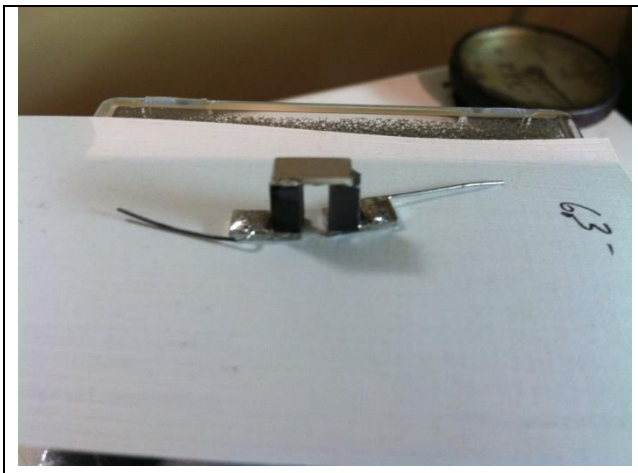

Figure 25 Silicide based TEPG devices fabricated using setup shown in Figure 24.

Characterization

We characterized these devices using a simple method depicted in Figure 26. This method provides information on the combined Seebeck coefficient of the n-type and p-type legs of the device, the internal resistance of the device and the power generated at a given temperature difference between the hot and cold side. Figure 27 shows the test set up of the device arrangement and Figure 28 shows a close up view of Figure 27.

Device measurements and corresponding characterization results for Sample 1 and Sample 3 (each are single TEPG devices) are shown in Tables 4 and 5, and Figures 29 and 30. Device measurements and corresponding characterization results for Sample 4 (a double TEPG device) are shown in Table 6 and Figure 31.

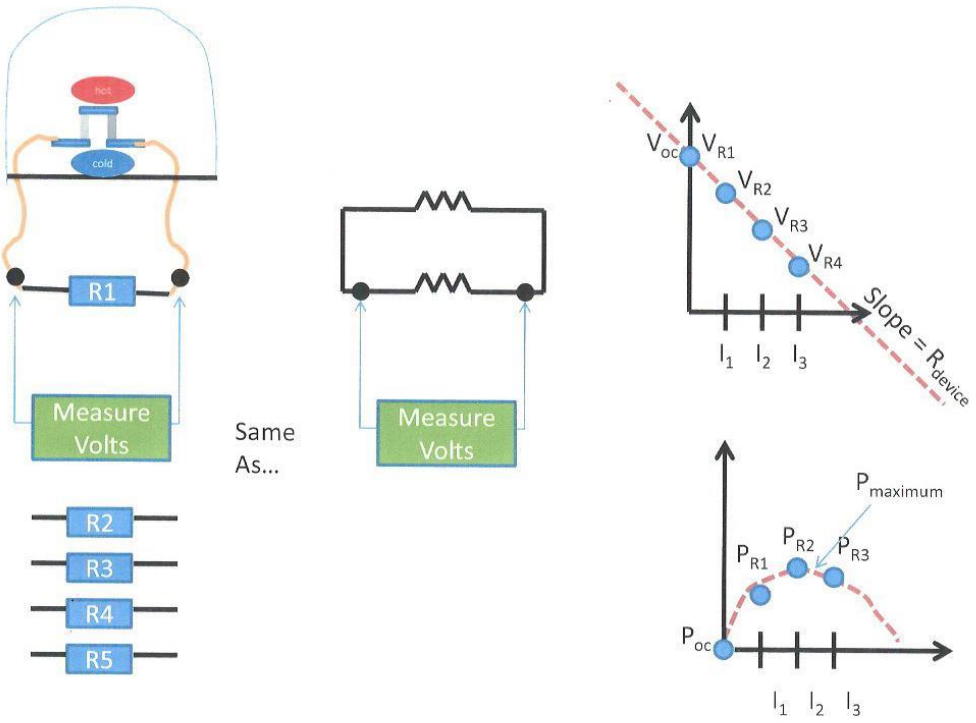

Figure 26. Method used to characterize TEPG devices.

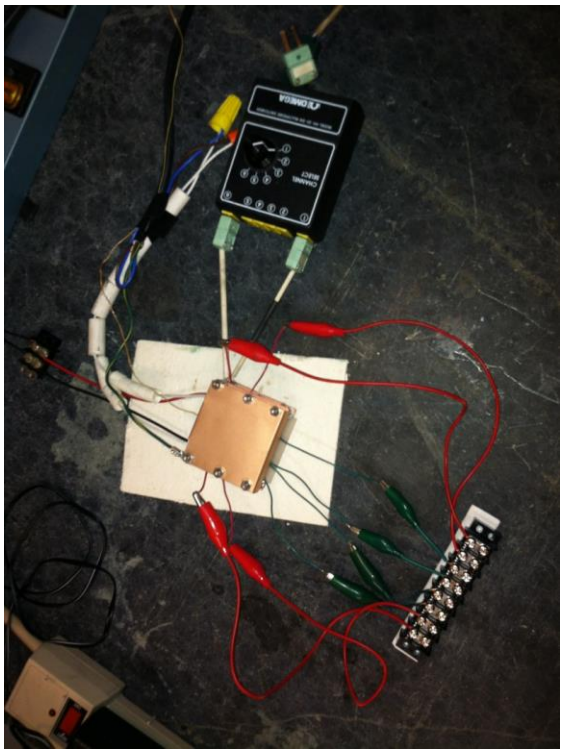

Figure 27. Set-up for measurement of properties of TEPG device.

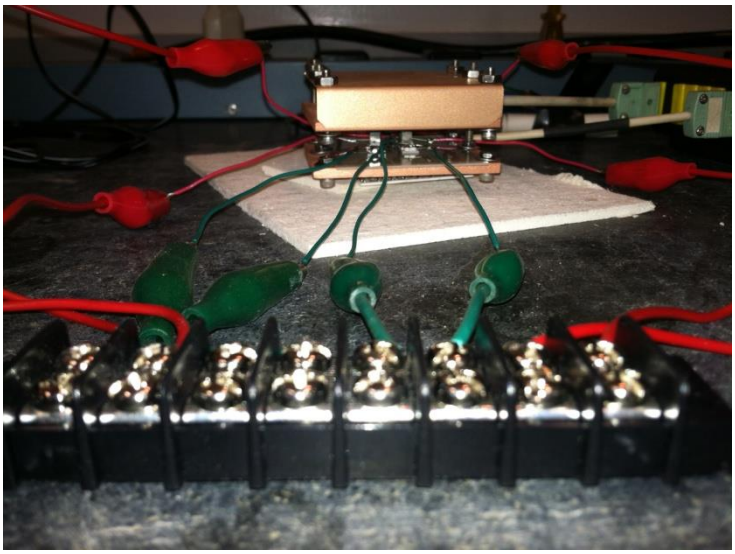

Figure 28. Close up view of the set-up shown in Figure 27.

Table 5 shows measurements on Device # 1 and Figure 29 shows the plot of the voltage drop across the standard resistance versus current, the slope of which provides the internal resistance of the device.

Table 5. Measurements on Device #1					
Sample 1	Reading 1				
Resistance Ω	Low °C	High °C	ΔT	Voltage mV	Current mA
0.00	41	100	59	10.035	#DIV/0!
0.60	41	100	59	6.06	10.100
0.05	41	100	59	1.16	23.200
0.02	41	100	59	0.528	26.400
0.00	57	150	93	15.77	#DIV/0!
0.60	57	150	93	9.8	16.333
0.05	57	150	93	1.829	36.580
0.02	57	150	93	0.816	40.800
0.00	73	204	131	24.4	#DIV/0!
0.60	73	204	131	14.61	24.350
0.05	73	204	131	2.72	54.400
0.02	73	204	131	1.22	61.000
0.00	90	248	158	32.11	#DIV/0!
0.60	90	248	158	19.04	31.733
0.05	90	248	158	3.56	71.200
0.02	90	248	158	1.6	80.000
0.00	121	302	181	40.2	#DIV/0!
0.60	121	302	181	23.62	39.367
0.05	121	302	181	4.41	88.200
0.02	121	302	181	1.99	99.500

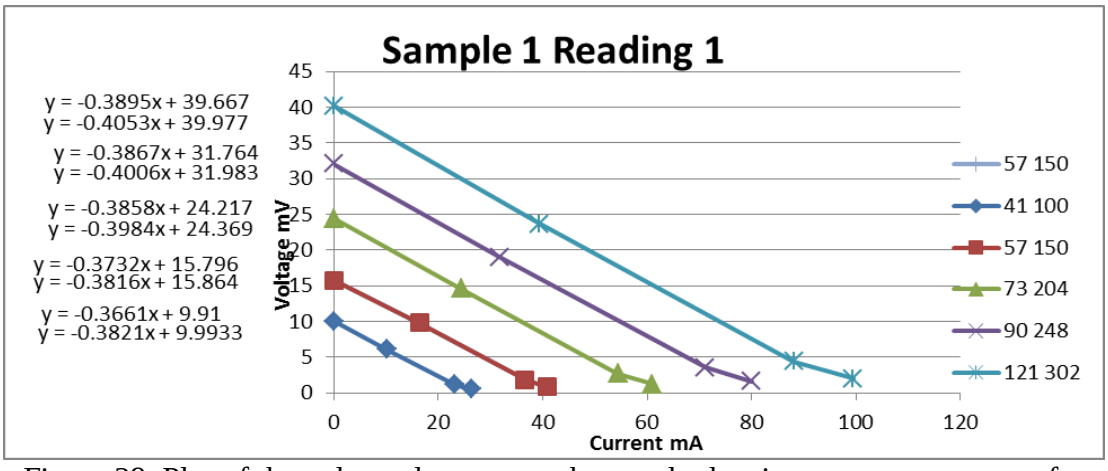

Figure 29. Plot of the voltage drop across the standard resistance versus current for Sample #1

Analysis of TEPG Devices

A good indicator of a materials quality can be obtained by determining the combined Seebeck coefficient. To determine the combined Seebeck coefficient, the open-circuit voltage (V_{oc}) is plotted as a function of the temperature difference (Figure 32). The data plots as a straight line. The best fit to this line is the sum of the Seebeck coefficient of the n-type and p-type legs of the device. For our data, this works out to be about 240 microvolts/K which shows that each leg has roughly 120 microvolts/K on average, which is quite respectable.

The plots of current and voltage data (slope) on the first device show that *the internal device resistance is very high,* about 350 to 400 mOhm. It can also be seen from the plot that the internal device resistance remains constant with the temperature. The resistance of the device should increase with temperature due to acoustic-mode scattering of the lattice - it should have a power-law dependence with exponent of three-halves.

Referring back to Tables 3 and 4 indicate that the resistance of the n-type and p-type legs were in the range of 1 to 7 mOhm at room temperature. This clearly indicates that the extra resistance is not reflective of the material. The fact that there is no change in resistance means that it could be a bad contact or a series resistance term from the wires. But from the Seebeck Coefficient analysis above, we know that the material is good.

Given these results, we then decided to measure open circuit voltage at various temperature differences between hot and cold end of all three devices. Tables 6-8 show Voc at various delta T for each of this device and the corresponding plots are shown in Figures 30-31. These plots show that Voc versus delta T are a straight line.

One thing we observe is that the Voc versus temperature difference plot has the y-intercept. It appears in all plots (Figure 31 to Figure 33) that there is always a voltage offset of some negative voltage when delta-T goes to zero. It is probably the fact that these devices operate at high temperature and the measurements are taken at low T. So there is probably a non-linearity near delta-T of zero.

Table 6. Open Circuit Voltage vs Delta T for Sample #1

Sample 1	Reading 1		Reading 2		
ΔT	Voltage mV	Voltage μV	ΔT	Voltage mV	Voltage μV
59	10.035	10035	56	10.038	10038
93	15.77	15770	93	17.03	17030
131	24.4	24400	126	24.87	24870
158	32.11	32110	157	32.51	32510
181	40.2	40200	181	40.28	40280

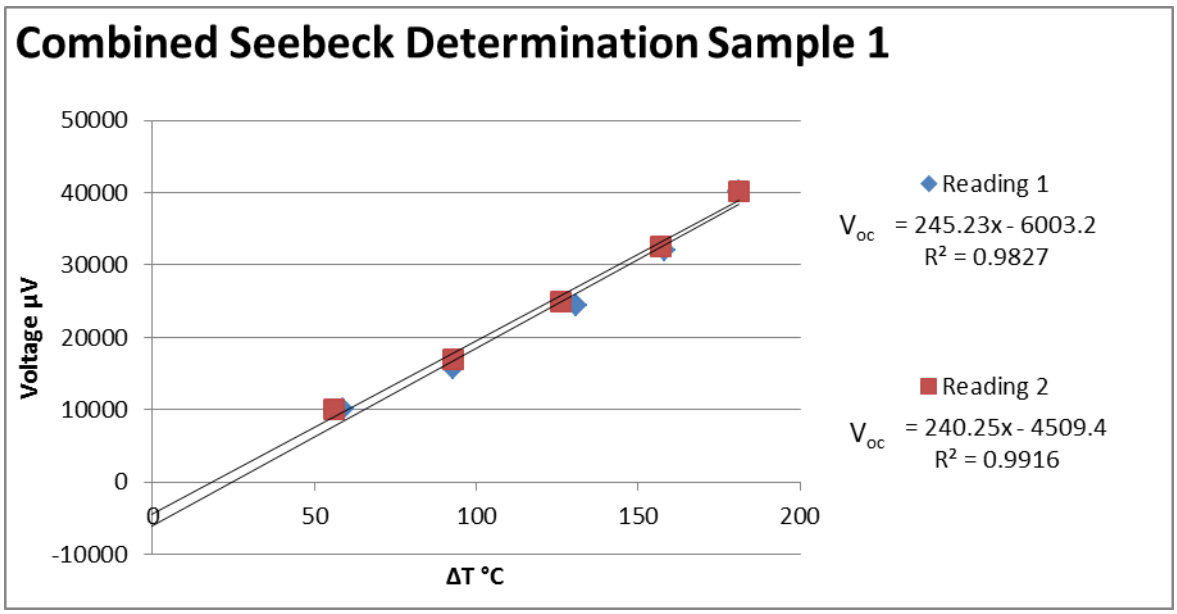

Figure 30. Combined Seebeck Determination for Sample #1.

Table 7. Open Circuit Voltage vs Delta T for Sample #3

Sample 4	Reading 1		Reading 2		
ΔT	Voltage mV	Voltage µV	ΔT	Voltage mV	Voltage µV
56	10.038	10038	59	10.035	10035
93	17.03	17030	93	15.77	15770
126	24.87	24870	131	24.4	24400
157	32.51	32510	158	32.11	32110
181	40.28	40280	181	40.2	40200

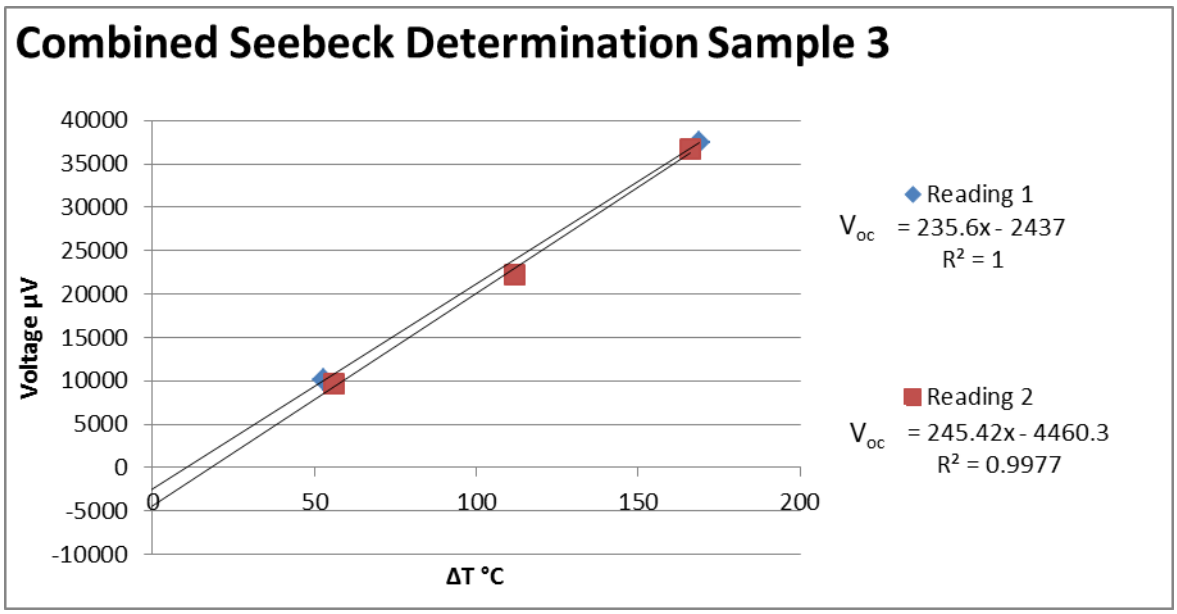

Figure 31. Combined Seebeck Determination for Sample #3.

Table 8. Open Circuit Voltage vs Delta T for Sample #4.

Sample 3	Reading 1		Reading 2		
ΔT	Voltage mV	Voltage µV	ΔT	Voltage mV	Voltage µV
53	10.05	10050	56	9.65	9650
	23.89	23890	112	22.28	22280
169	37.38	37380	166	36.66	36660

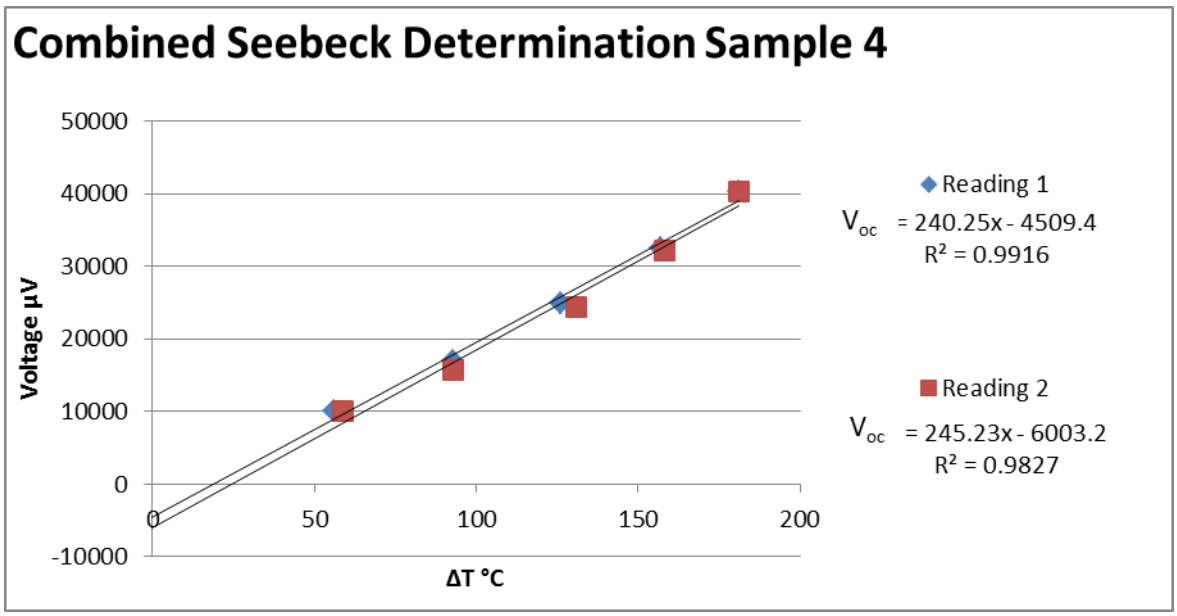

Figure 32. Combined Seebeck Determination for Sample #4.

The measurements of resistance and resistivity coupled with the Seebeck coefficient data indicate that **we have a very good thermoelectric material**, and the problem is with contacts. We are going to carry out the measurements with newly fabricated devices/ contacts and present the results in Phase II proposal.

Hence during Phase II proposal we will focus on to the following tasks:

1. Develop an optimized process for reproducibly obtaining low resistance electrical contacts. (Use both In-Ni and Sn-Ni system and use of a monobloc sintering method using FAST),
2. Measuring the electrical contact resistance for bulk legs using a scanning needle probe,
3. Developing a dedicated test system for devices where the series resistance can be minimized for all tests,
4. Measuring thermal conductivity using technique we used earlier on other thermoelectric materials [33].

4.6 Investigation of Thermal Management

The magnitude of the power generated by a TEPG device is dependent on temperature difference between the hot and cold end of the device. This makes the effective coupling of waste heat at the hot end and effective passive dissipation at colder end very important. In turn this makes thermal management very important for TEPG technology. In collaboration with ARL/PSU we had a small effort investigating light weight composites with good thermal conductivity for thermal management.

Significant progress has been in improving the thermal conductivity of copper by incorporating diamond particles in the matrix of copper alloy. It has been demonstrated that copper matrix should have small volume fraction of strong carbide forming elements such as Ti or Zr. These

elements interact with diamond during the sintering process and a thin layer of carbide such as TiC or ZrC is form between the diamond and copper matrix, thus enhancing the heat transfer phenomena (Figure 33)

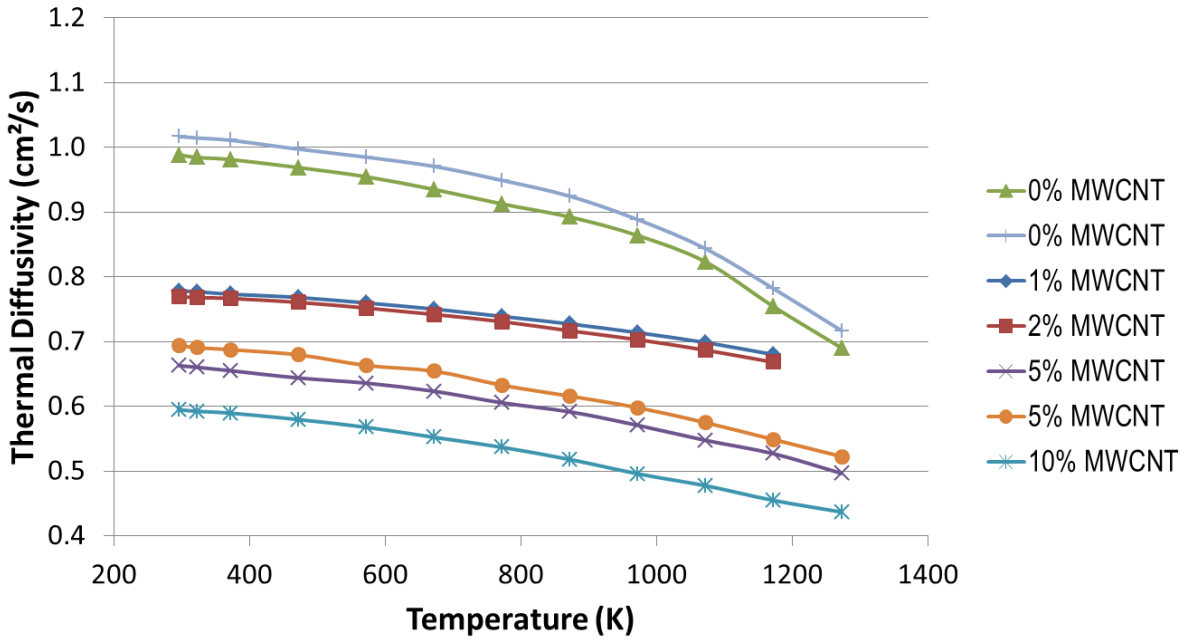

Figure 33: Thermal Diffusivity of copper alloy with various volume fractions of carbon nanotubes (CNTs).

Since copper is a high density material (density 8.96 g/cc), effort is underway in looking for light-weight materials such as Al-based alloy (2.7 g/cc). Preliminary effort has demonstrated that the thermal conductivity of Al (238 W/mK) could be enhanced by incorporating flakes of thermal grown pyrolitic graphite (TEPG) material that has good thermal conductivity (i.e., 1600 W/mK) in the planar direction. Al powder was blended with different volume fractions of TEPG flakes and sintered by field assisted sintering process. Figure 32 shows that the thermal conductivity of Al material was increased from 238 W/mK to 850 W/mK by incorporating about 75 volume % of TEPG flakes in the planar direction. These flakes were aligned in one direction that was perpendicular to axial sintering pressure (Figure 34). Cross section photographs show that these flakes have limited connectivity with each other and aligned in one direction. In spite of limited connectivity of flakes, heat transfer, i.e., directional thermal conductivity of Al-composite, is very attractive (850 W/mK) as compared to base line or what has been reported in the literature for Al alloy. This work was jointly done by Penn State University and Momentive Co., Cleveland, OH. Following this we are further enhancing thermal conductivity by having some connectivity between flakes that could be achieved by incorporating carbon nanotubes (CN) in the composite. CN also has thermal conductivity ranging 1500 to 3000 W/mK depending on its quality. Effort is underway in sintering Al powder with small volume fraction of CN and TEPG flakes with the anticipation that CN will enhance the connectivity between flakes.

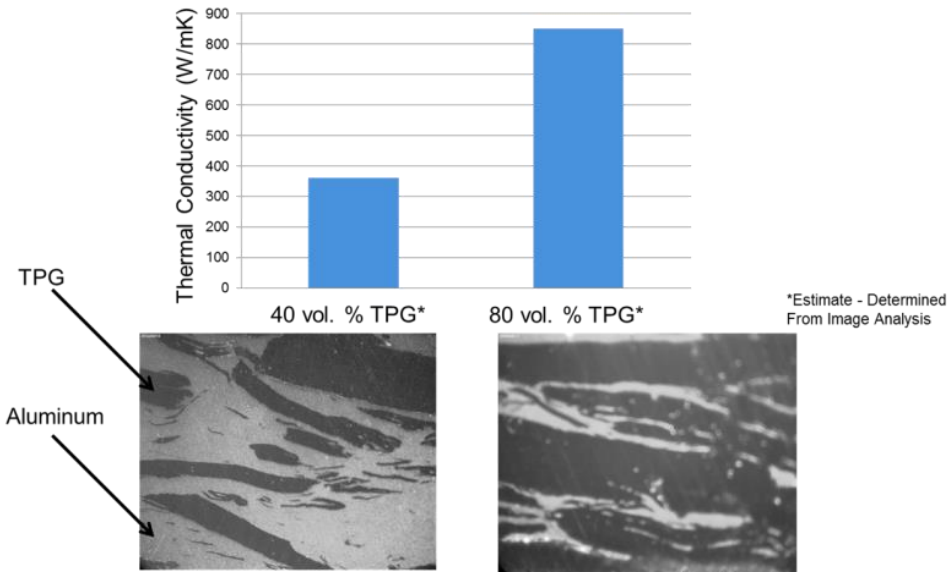

Figure 34. Thermal conductivity of Al with various volume fraction of TEPG flakes and corresponding cross section microstructure.

5. Conclusions and Future Plans

During Phase I of this work we spent a great deal of effort on the material technology issues. We successfully produced Mg_2Si and MnSi material with good thermoelectric properties. We developed suitable techniques to synthesize Mg_2Si with good crystalline quality. We produced n-type Mg_2Si and p-type MnSi nanocomposite pellets using FAST. X-ray diffraction measurements confirmed that the materials were stoichiometric, and optical micrographs revealed that they were fully dense with little porosity. Each surface was electrochemically coated with nickel, and the material was cut into n and p type legs. The legs showed good resistivity and were then used to fabricate several TEPG devices. Measurements of resistivity and voltage while the device was subjected to a temperature gradient indicated a combined Seebeck coefficient of 240 μV/K, or roughly 120 μV/K on average per leg, which is quite respectable. Given these results, we are on track to develop materials with ZT on the order of 1.6 or higher.

In future work, we plan to:

- Perform modeling work to investigate the possibility of improving the Seebeck coefficient of the material. Although it has always been believed that Seebeck coefficient is a given parameter for a material, we believe it may be possible to manipulate it in nanocomposite materials.
- Develop p-type magnesium silicide so that both legs of the TEPG device will be the same which will minimize thermal
- Scale up the technique for production of thermoelectric silicides.
- Systematically evaluate the effect of metallic binders on the thermal conductivity and thermoelectric performance

- Develop an optimized process for reproducibly obtaining low resistance electrical contacts. (Use both In-Ni and Sn-Ni system and use of a monobloc sintering method using FAST)
  Measuring the electrical contact resistance for bulk legs using a scanning needle probe.
  Developing a dedicated test system for devices where the series resistance can be minimized for all tests.
  Measuring thermal conductivity using technique we used earlier on other thermoelectric materials.
- Explore extrusion as opposed to the FAST technique to produce the TE materials.
- Explore segmented devices and coatings to prevent degradation.

6. References

[1] Dresselhaus, M. S. et al. New directions for low-dimensional thermoelectric materials. Adv. Mater. **9,** 1043–1053 (2007).

[2] Chen, G., Dresselhaus, M. S., Dresselhaus, G., Fleurial, J. P. & Caillat, T. Recent developments in thermoelectric materials. Int. Mater. Rev. **48,** 45–66 (2003).

[3] G. Joshi, H. Lee, Y. Lan, X. Wang, G. Zhu, D. Wang, R. W. Gould, D. C. Cuff, M. Y. Tang, M. S. Dresselhaus, G. Chen, and Z. Ren, Nano Lett. 8,4670 (2008).

[4] B. Poudel, Q. Hao, Y. Ma, Y. Lan, A. Minnich, B. Yu, X. Yan, D. Wang,A. Muto, D. Vashaee, X. Chen, J. Liu, M. S. Dresselhaus, G. Chen, and Z.Ren, Science 320, 634 (2008).

[5] A. I. Hochbaum, R. Chen, R. D. Delgado, W. Liang, E. C. Garnett, M.Najarian, A. Majumdar, and P. Yang, Nature 451, 163 (2008).

[6] J. M. O. Zide, D. Vashaee, Z. X. Bian, G. Zeng, J. E. Bowers, A. Shakouri, and A. C. Gossard, Phys. Rev. B 74, 205335 (2006).

[7] J. P. Heremans, C. M. Thrush, and D. T. Morelli, J. Appl. Phys. 98, 063703 (2005).

[8] J. P. Heremans, V. Jovovic, E. S. Toberer, A. Saramat, K. Kurosaki, A. Charoenphakdee, S. Yamanaka, and G. J. Snyder, Science 321, 554(2008).

[9] C. M. Jaworski, V. Kulbachinskii, and J. P. Heremans, Phys. Rev. B 80, 233201 (2009).

[10] O. Rabin, Y.-M. Lin, and M. S. Dresselhaus, Appl. Phys. Lett. 79, 81 (2001).

[11] T. Koga, X. Sun, S. B. Cronin, and M. S. Dresselhaus, Appl. Phys. Lett.73, 2950 (1998).

[12] A. J. Minnich, M. S. Dresselhaus, Z. F. Ren, and G. Chen, Energy Env. Sci. 2, 466 (2009).

[13] C. J. Vineis, A. Shakouri, A. Majumdar, and M. G. Kanatzidis, Adv.Mater. 22, 3970 (2010).

[14] John Fairbanks, 'Automotive Thermoelectric Generators and HVAC, Presentation and Talk at 2013 Annual Merit Review and Peer Evaluation Meeting DOE Vehicle Technologies Office.http://www4.eere.energy.gov/vehiclesandfuels/resources/merit-review/sites/default/files/ace00e_fairbanks_2013_o.pdf

[15] Seijiro Sano, Hiroyuki Mizukami, Hiromasa Kaibe, "Development of High-Efficiency Thermoelectric Power Generation System," Komatsu Technical Report, Vol.49, No. 152 (2003)

[16] Tatsuya Sakamoto, Tsutomu Iida, Atsunobu Matsumoto, Yasuhiko Honda, Takashi Nemoto, Junichi Sato, Tadao Nakajima, Hirohisa Taguchi, and Yoshifumi Takanashi. "Thermoelectric Characteristics of a Commercialized Mg_2Si Source Doped with Al, Bi, Ag, and Cu." Journal of Electronic Materials. Vol 39, No. 9, 2010.

[17] M.J. Yang, L.M. Zhang, L.Q.Han, Q. Shen and C.B. Wang. Indian Journal of Engineering and Materials Sciences, Vol. 16, August 2009, pp. 277-280.

[18] J.P. Fleurial, P. Gogna, G.Chen, M.S. Dresselhaus, H. Lee, M.Y. Tang, Z.F. Ren, D. Wang, S. Bux, D. King, R. Kaner, and R. Blair. "Nanostructured Bulk Thermoelectric Materials" http://ect2008.icmpe.cnrs.fr/Contributions/I-05-Fleurial.pdf.

[19] K.Ono and R.O. Suziki. J. of Materials, Energy Resources Overview. December 1998, p49.

[20] Sabah K. Bux, Michael T. Yeung, Eric S. Toberer, G. Jeffrey Snyder, Richard B. Kaner and Jean-Pierre Fleurial. "Mechanochemical synthesis and thermoelectric properties of high quality magnesium silicide" ***J. Mater. Chem.***, 2011, **21**, 12259-12266.

[21] "Alternative Green Technology For Power Generation Using Waste-Heat Energy And Advanced Thermoelectric Materials," NASA STTR Phase I Contract #NNX11C134P, 2/18/11 – 2/18/12, Phase II Contract**:** NNX12CB08C, June 15, 2012 – June 15 2014. Monitored by NASA Langley Research Center. POC: Dr. Narasimha Prasad (757-864-9403)

[22] Narasimha S. Prasad, Sudhir B. Trivedi, Witold Palosz, Sue Kutcher, Robert Rosemeier, Cory Rosemeier, Patrick J. Taylor, Jay Maddux, Jogender Singh. *Proceedings of SPIE* Volume 8377. 23 - 24 April 2012.

[23] S. Trivedi, P. Taylor, and W. Sarney, "Refractory, Low-Resistance Electrical Contact Technology", ARL Patent Docket# ARL-10-08. (Spring 2010).

[24] Zaitsev ,V K, Fedorov M I, Eremin I S and Gurieva E A 2006 Thermoelectrics Handbook: Macro to Nano-Structured Materials ed. CRC Press (New York) ch. 29

[25] J. Soga, T. Iida, Y. Higuchi, T. Sakuma, K. Makino, M. Akasaka, T. Nemoto* and Y. Takanashi, *Thermoelectrics, 2005. ICT 2005. 24th International Conference on*, pp.95-98, 19-23, June 2005.

[26] Final Report to AFOSR DURIP (FA9550-06-1-0326), MURI "Energy Harvesting and Storage Systems for Future AF Vehicles", University of Washington:Minoru Taya (PI),(2012)

[27] U.A. Tamburini, J.E. Garay and Z.A. Munir, Scripta Materialia, **54** (2006), 823 – 828.

[28] "Synthesis of Thermoelectric Manganese Silicide by Mechanical Alloying and Pulse Discharge Sintering," T. ITOH and M. YAMADA, Journal of Electronic Materials 38(7) (2009)925-929.

[29] "Rapid synthesis of high thermoelectric performance higher manganese silicide with in-situ formed nano-phase of MnSi," Intermetallics 19(2011) 404-408.

[30] K. Arai, K. Nishio, N. Miyamoto, K. Sunohara, T. Sakamoto, H. Hyodo, N. Hirayama, Y. Kogo and T. Iida, "Fabrication of Mg_2Si bulk by spark plasma sintering method with Mg_2Si nano-powder," Mater. Res. Soc. Symp. Proc. Vol. 1490 © 2010 Materials Research Society pp. 63-68.

[31] Y. Hayatsu, T. Iida, T. Sakamoto, S. Kurosaki, K. Nishio, Y. Kogo, and Y. Takanashi, "Fabrication of large sintered pellets of Sb-doped N-type Mg_2Si using a plasma activated sintering method," AIP Conference Proceedings 1449, 187-190 (2012).

[32] Kyung-Ho Kim, Soon-Mok Choi, and Won-Seon Seo, Il-Ho Kim, Sun-Uk Kim, "Synthesis Characteristics and Thermoelectric Properties of the Rare-Earth-Doped Mg_2Si System" Journal of Korean Physical Society, Vol. 57, No. 4, October 2010, pp. 1072_1076.

[33] Patrick J. Taylor, Jay R. Maddux,Sudhir B. Trivedi. "Isothermal method for rapid, steady-state measurement of thermoelectric materials and devices," Paper 8035-40 of Conference 8035, 27 April 2011.

[34] Tatsuya Sakamoto, Tsutomu Iida, Shota Kurosaki, Kenji Yano, Hirohisa Taguchi, Keishi Nishio and Yoshifumi Takanashi. Journal of Electronic Materials, Volume 40, Issue 5, May 2011, pp 629-634.